DEVELOPMENT OF ANTIBACTERIAL POLYMER BASED NANOCOMPOSITE MATERIALS

A Thesis Submitted to
the Graduate School of Engineering and Sciences of
İzmir Institute of Technology
in Partial Fulfillment of the Requirements for the Degree of

MASTER OF SCIENCE

in Biotechnology

by
Ezgi ABATAY

March 2015
İZMİR

We approve the thesis of **Ezgi ABATAY**

Examining Committee Members:

_____

Assist. Prof. Dr. Alper ARSLANOĞLU
Department of Molecular Biology and Genetics, İzmir Institute of Technology

_____

Asisst. Prof. Dr. Engin ÖZÇİVİCİ
Department of Mechanical Engineering, İzmir Institute of Technology

_____

Assist. Prof. Dr. Sevgi KILIÇ ÖZDEMİR
Department of Chemical Engineering, İzmir Institute of Technology

16 March 2015

_____

Assist. Prof. Dr. Alper ARSLANOĞLU
Supervisor, Department of Molecular Biology and Genetics, İzmir Institute of Technology

_____

Prof. Dr. Metin TANOĞLU
Co-Supervisor, Department of Mechanical Engineering, İzmir Institute of Technology

_____

Prof. Dr. Volga BULMUS
Head of the Department of Biotechnology and Bioengineering

_____

Prof. Dr. Bilge KARAÇALI
Dean of the Graduate School of Engineering and Sciences

ACKNOWLEDGMENTS

I would like to thank and express my deepest gratitude to my advisor, Assistant Professor Alper ARSLANOĞLU and my co-advisor Prof. Metin TANOĞLU for their invaluable advice, guidance, support and encouragement.

I would like to thank the Center for Materials Research staff at Izmir Institute of Technology for their help and patience during my study.

I would like to acknowledge industrial theses support program (SAN-TEZ) for financial support to 1209-STZ.2012-1 project for their support to my study.

I would like to thank to Mert Ol, Berna NALBANT and Aslı KIRIMŞELİOĞLU from AKG Yalıtım ve İnşaat Malzemeleri San. ve Tic. A.Ş. for providing the materials and the mechanical test machines, also for their advice throughout my study.

I am especially grateful to my laboratory colleagues for their encouragement, help and patience.

Special thanks to my family and Research Assistant Osman KARTAV for their endless understanding, supports, motivation, continuous advice and love in all my life and believing in me. I am always sure that they are happy to be there for me. I cannot even imagine how much they contribute efforts for me.

ABSTRACT

DEVELOPMENT OF ANTIBACTERIAL POLYMER BASED NANOCOMPOSITE MATERIALS

Human beings are often infected by microorganisms such as bacterium, mold, yeast, virus, etc. in the living environment. It became a requirement and a necessity to create sterile fields in areas. Composite stones are one of the main materials that can be used for the contact surfaces in indoor and outdoor places due to their being of highly resistant to abrasives, chemicals and impacts. Research has been intensive in antibacterial material containing various inorganic substances.

The aim of this thesis is investigating the antibacterial effect of inorganic substances such as silver, zinc oxide, calcium oxide, titanium oxide and magnesium oxide on stone products. This study also deals with the silver doped zinc oxide powder and their antibacterial efficacies.

Stone product is formed of mainly two type compound which are quartz aggregates as reinforced and filler and thermoset polyester resin as matrix. The manufacturing process begins with selection of raw quartz materials. They are crushed and blended in the ratio of 90 % quartz aggregates to 10% polyester matrix and other additives such as antibacterial agent, pigment. These united constituents are used for production of composite stones by applying those combined vacuum, vibration and pressing processes which are named as vibropress, simultaneously. Following it, they are subjected to surface preparation and polishing processes.

In this study, mechanical, thermal, and morphological properties of the particles, polyester matrix and stone product were investigated. Antibacterial efficacies of these were investigated based on colony-count method against gram negative (E.coli) and gram positive (Bacillus subtilis) bacteria. Silver-containing stone samples showed best antibacterial property about ninety-nine percent reduction.

ÖZET

ANTİBAKTERİYEL POLİMER ESASLI NANOKOMPOZİT MALZEMELERİN GELİŞTİRİLMESİ

İnsanlar bakteri, küf, maya, virüs gibi mikroorganizmalar tarafından sıklıkla enfekte edilir. Bu yüzden steril alanları oluşturmak zorunluluk ve gereklilik haline gelmiştir. Kompozit taşlar; aşındırıcılar, kimyasallar ve darbelere karşı son derece dayanıklı olmaları nedeni ile kapalı ve açık mekanlarda temas eden yüzeylerde kullanılabilen ana malzemelerden biridir. Araştırmalar çeşitli inorganik maddeler içeren antibakteriyel malzemeler üzerine yoğunlaşmıştır.

Bu tezin amacı, taş üzerindeki gümüş, çinko oksit, kalsiyum oksit, titanyum oksit ve magnezyum oksit gibi inorganik maddelerin antibakteriyel etkisini araştırmaktır. Bu çalışma aynı zamanda gümüş katkılı çinko oksit tozu ve antibakteriyel etkinlikleri ile ilgilenir.

Kompoze taş, matris olarak ısıyla sertleşen poliester reçine dolgu ve takviye amaçlı olarak kuvars agregalardan oluşan başlıca iki tip bileşenden oluşturulur. Üretim süreci ham kuvars malzemelerinin seçimi ile başlar. % 10 poliester resin, antibakteriyel ajan, ve pigment gibi katkı maddeleri, kuvars agregaları ile % 90 oranında karıştırılır. Bu birleşik bileşenler, vibropres olarak adlandırılan presleme işlemi, birleşik vakum, presleme ve titreşim aynı zamanda uygulanarak kompozit taşların üretimi için kullanılmaktadır. Bunu takiben, bu taşlar yüzey hazırlama ve parlatma süreçlerine tabi tutulur.

Bu çalışmada, partiküllerin, polyester matrisin ve üretilen taşın morfolojik, termal ve mekanik özellikleri incelenmiştir. Bunların antibakteriyel etkinlikleri gram negatif (E. coli) ve gram pozitif (Bacillus subtilis) bakterilerine karşı koloni sayım yöntemi baz alınarak incelenmiştir. Gümüş içeren taş örnekleri yaklaşık yüzde doksan dokuz bakteriyel azalma ile en iyi antibakteriyel özelliği göstermiştir.

TABLES OF CONTENTS

LIST OF FIGURES

Figure **Page**

LIST OF TABLES

Table **Page**

CHAPTER 1

INTRODUCTION

Environmental and air pollution become serious problems for human health because of industrialization and urbanization. This situation causes to exist more microorganisms which are found everywhere, in air, soil and water. Therefore contamination by microorganisms is of great concern in a variety of areas such as medical devices, healthcare products, water purification systems, hospitals, dental office equipment, food packaging, food storage, household sanitation, textiles etc. Infections by pathogenic microorganisms are responsible for diseases among people, animals and plants. Generally the infections are produced by touching, eating, drinking or breathing (Muñoz-Bonilla and Fernández-García 2012). The main problem to eliminate microorganisms is that their genes mutate rapidly and easily and make them resistant.

Bacteria can be classified by their ability to retain the gram stain (gram positive or gram-negative) and by the shape of the individual organisms (cocci, bacilli, curved or spiral). One distinction is done based on gram stain. According to gram stain technique, first procedure requires fixing the cells by heating. Crystal violet which is basic dye is added so all bacteria will stain purple. Next, iodine and ethanol is added, respectively. Gram-positive cells remain purple, while gram-negative cells become transparent. Finally, gram-positive cells are still purple although gram-negative cells are red by effect of counterstaining with safranin (Michael L. Shuler 2002).

Bacillus subtilis is a typical gram- positive cell which do not have an outer membrane. It only include inner membrane having very thick, rigid cell wall with multiple layers of peptidoglycan and teichoic acids covalently bonded to the peptidoglycan.

Gram-negative cell has two membrane. Outer membrane supported by a thin peptidoglycan layer. Peptidoglycan which is polysaccharide with amino acids shows chain-link fence structure. A inner membrane which contains about 50% protein, 30% lipids and 20% carbohydrates is separated from the outer membrane by periplasmic space (Michael L. Shuler 2002). The cell envelope serves to protect important cellular compounds and to preferentially exclude undesirable compounds in the environment.

Loss of membrane integrity leads to cell lysis and cell death. Escherichia coli (E.coli) is a typical gram-negative cell which is the one of the most exposed bacteria because it spreads out with drinking water and causes urinary tract infection, newborn meningitis, sepsis, hemolytic uremic syndrome (Orsi 2007). Also another bacteria Pseudomonas aeruginosa is the main reason for infections which effects human health directly and it increasingly gains strength for many antibiotics (Muñoz-Bonilla and Fernández-García 2012). Because of these reasons there is a definite need for antibacterial materials. Antibacterial polymers are most suitable and effective materials for antibacterial activity and production of polymers with antibacterial property becomes very important for industry (Kenawy 2007). There are very rapid developments in research for polymer nanocomposites because they have many advantages for industry and wide application area. Polymer nanocomposites is a polymer that has been reinforced with small quantity of nano-sized inorganic particles such as quartz, aramid, polyethylene, polybenzoxazole (Tan, Tay, and Teo 2005, Srivastava, Majumdar, and Butola 2012). By the usage of nanosized inorganic particles into polymer matrices, the material will show new and unexpected properties and it become totaly different from conventional materials. Physical properties are improving with addition of nanosized particles such as strenth, heat resistance and modulus of elasticty (Tan, Tay, and Teo 2005, Srivastava, Majumdar, and Butola 2012).

Recently, there has been very rapid development of producing antibacterial polymers. Polymer nanocomposites gain antibacterial property by addition of metal nanoparticles such as silver (Ag), gold (Au), zinc oxide (ZnO), titanium dioxide (TiO_2), alumina (Al_2O_3) and iron oxides (Fe_3O_4, Fe_2O_3) (Emamifar 2011).

Antimicrobial agents can be effective on bacteria through two ways: bacteriostatic (bacteria-inhibiting) and bactericidal (bacteria-killing) actions. If an antibacterial agent is bacteriostatic, bacteria will resume growth upon removal of the agent. Bacteriostatic agent is only inhibit or prevent bacterial growth. However, bactericidal action which is an irreversible action kills the bacteria and destroys the microorganism in such a way that the reproduction is no longer possible. In fact, these bactericidal agents can be examined through five possible mechanisms; the damaging of DNA, the denaturation of proteins, the disruption of cell wall or membrane, the removal of free sulfhydryl groups, and the chemical antagonism defined as inactivation of the enzymes. Because of the wide usage and properties of metal nanoparticles many

investigators have studied metal nanoparticles. Silver is the most useful nanoparticle because of its unique electric, optical, catalytic and antimicrobial properties (Dallas, Sharma et al. 2011).

The antimicrobial properties of silver have been known to cultures all around the world for many centuries. Silver is a strong agent that is capable of killing 650 organisms which causes infections (Jeong et al. 2005). Therefore silver has the potential to be an excellent antibacterial agent. The silver that has been mainly used for antibacterial finishing during the past few decades (Qian, Yin et al. 2001). As technologies for producing nanoparticles have developed to a high-degree recently, attempts have been made to apply them to antibacterial finishing. As the size of the silver particles decreases, down to the nano-scale regime, their antibacterial efficacy increases because of their larger total surface area per unit volume (Jeong et al. 2005). Although silver shows strong toxicity toward a broad range of microorganisms, collodial silver is relatively safe for humans, plants and allmulti-celled livingmatter. Therefore silver is probably the most powerful antimicrobial agent comparing to all other available antimicrobial agents (Dallas, Sharma et al. 2011). Various mechanisms of silver's effect depends on the concentration of free Ag^{+2} ions. The mechanism of the antimicrobial activity of silver particles has not fully been understood, however three most common mechanisms proposed are:

- Gradual release of free silver ions, followed by distruption of ATP production and DNA replication.
- Silver nanoparticles silver direct damage to cell membranes
- Silver nanoparticles and silver ion generation catalyze between reactive oxygen species in the cell and hydrogen atoms of thiol groups (Kim, Kuk et al, 2007; Inoue, Hoshino et al. 2002).

It is hypothesized that silver ions can interact with phosphorus moieties in DNA, resulting in inactivation of DNA replication. It is also suggested that silver atoms can react with sulfur-containing proteins in enzymes and subsequently leading to the inhibition of enzyme functions. S-Ag bands occur due to silver ions (particularly Ag^{+2}) released from silver nanoparticles in cell membrane. The bands occur with trans membrane energy generation and ion transport causes. The another mechanism is between hydrogen atoms of thiol groups and reactive oxygen species in the cell so by elimination of water molecules, covalently disulfide bond between two tyol group

occur. The silver-catalyzed formation of disulfide bonds can cause changes in protein structure and the inactivation of key enzymes (Davies and Etris 1997).

Reserch focus on the role of various nanoparticles as potential antimicrobials but low molecular weight antimicrobial agents have many disadvantages, such as toxicity to the environment and short-term antimicrobial ability. To overcome problems associated with the antimicrobial agents, antimicrobial functional groups can be introduced into polymer molecules (Kenawy, Worley, and Broughton 2007). The composites prepared using these nanoparticles and polymers can find better utilization due to the enhanced antimicrobial activity.

In this thesis, unsaturated polyester resin (UPR) and quartz aggregate was used to form one of the promising composite materials by mechanical mixing process. Also, silver (Ag), zinc oxide (ZnO), silver loaded zinc oxide (Ag/ZnO), titanium dioxide (TiO_2), magnesium oxide (MgO), and calcium oxide (CaO) particles was added to get antibacterial property for nanocomposite stones. Mechanical, thermal, and morphological properties of the powders, polyester resin and UPR-quartz stone product were investigated. Antibacterial efficacies of these powders and products were investigated based on colony-count method against gram negative (*Escherichia coli*) and gram positive (*Bacillus subtilis*) bacteria.

CHAPTER 2

LITERATURE REVIEW

Guzman et al. shows synthesis of Ag NPs prepared by chemical reduction from aqueous solutions of silver nitrate, containing a mixture of hydrazine hydrate and sodium citrate as reductants and sodium dodecyl sulfate as a stabilizer. They measure the antibacterial activity by the Kirby-Bauer method and they get reasonable bactericidal activity against *Escherichia coli*, *Pseudomonas aeruginosa*, and *Staphylococcus aureus* (Guzman, Dille, and Godet 2012). A schematically illusrated TEM image and particle size distributions of spherical Ag NPs is shown in Figure 2.1.

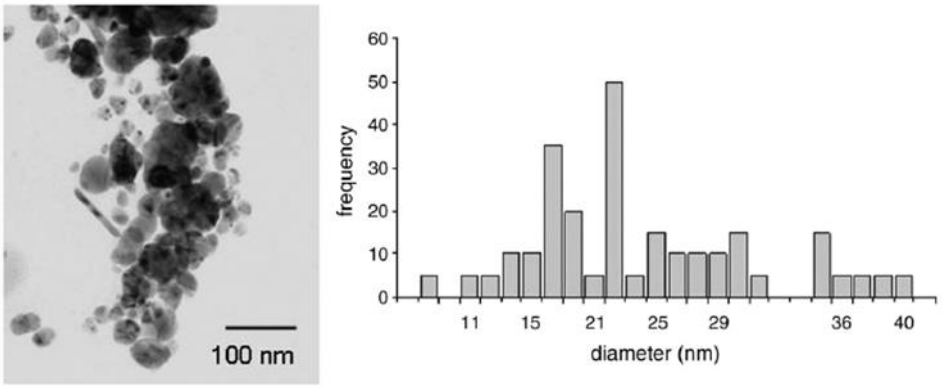

Figure 2.1. TEM image of spherical Ag NPs (left) and their particle size distributions (right). Ag NPs prepared from 1.1 mM AgNO3 solution (sample SHS-1) (Source: Guzman et al. 2012)

Sondi et al. investigate the antimicrobial activity of silver nanoparticles against *E. coli* as a model for Gram-negative bacteria. They use Scanning and transmission electron microscopy (SEM and TEM) study the biocidal action of this nanoscale material. Their results shows that investigated *E. coli* cells were damaged which show formation of "pits" in the cell wall of the bacteria (Sondi and Salopek-Sondi 2004). Scanning electron micrographs of native *E. coli* cells are shown in Figure 2.2.

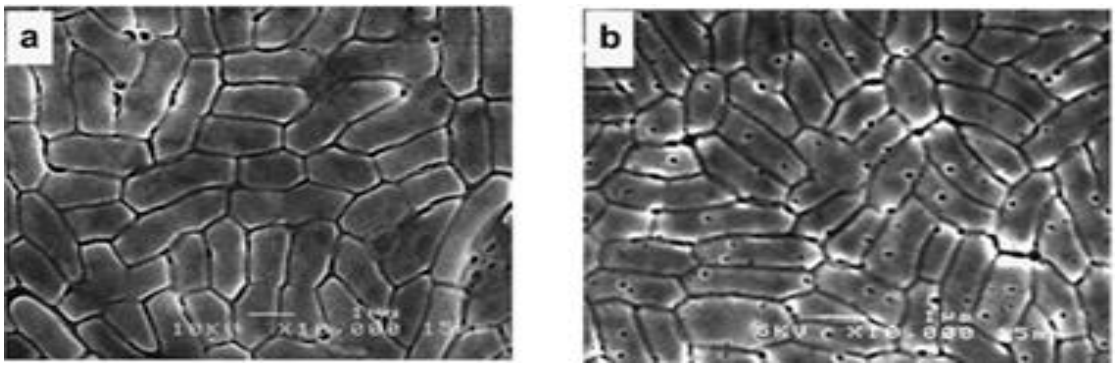

Figure 2.2. Scanning electron micrographs of native *E. coli* cells (a) and cells treated with 50 μg cm−3 of silver nanoparticles in liquid LB medium for 4 h (b) (Source: Sondi and Salopek-Sondi 2004)

Zibaii et al. investigate antimicrobial activity of the silver nanoparticles against Escherichia coli with using a nonadiabtic tapered fiber optic biosensor. With similar conditions for bacteria, the inhibition rate of the *E. coli* growth was measured by colony counting method as an experimental control and the results were compared with those obtained from the fiber sensor measurements. For colony counting the inhibition rates of the *E. coli* growth were measured to be from 1.27 h^{-1} to - 0.69 h^{-1} and for optical fiber biosensor from – 3.00×10^{-3} h^{-1} to - 1.98×10^{-2} h^{-1} (Zibaii et al. 2014). Diagram summarizing the interaction SNPs with bacterial cells are shown in Figure 2.3

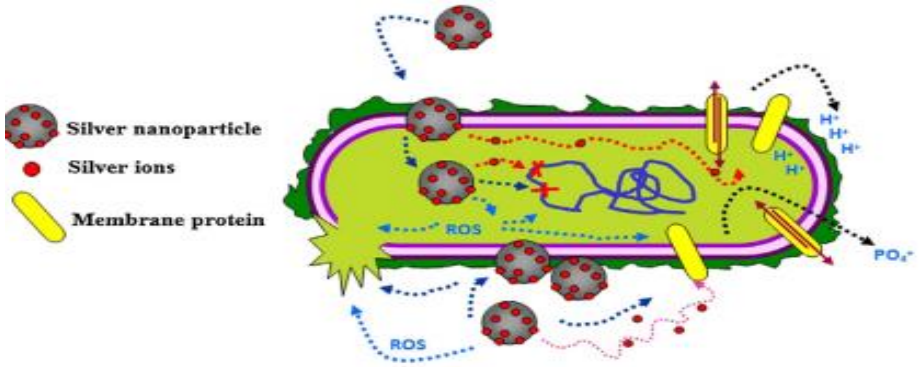

Figure 2.3. Diagram summarizing the interaction SNPs with bacterial cells. SNPs may (I) change membrane morphology and the bacterial cells incapable of correctly controlling transport through the plasma membrane; (II) interact with membrane proteins affecting their correct function; (III) enter into the cell where it can generate ROS, release silver ions, and affect DNA and inactivate of the enzymes bacteria (Source: Zibaii et al. 2014)

Raffi et al. investigated 16 nm mean size silver nanoparticles with estimating crystalline structure, morphology and nanoparticles size by X-ray diffraction (XRD) and transmission electron microscopy (TEM) (Raffi et al. 2008). TEM micrograph and XRD pattern of silver nanoparticles synthesized by inert gas condensation process are shown in Figures 2.4 and 2.5, respectively.

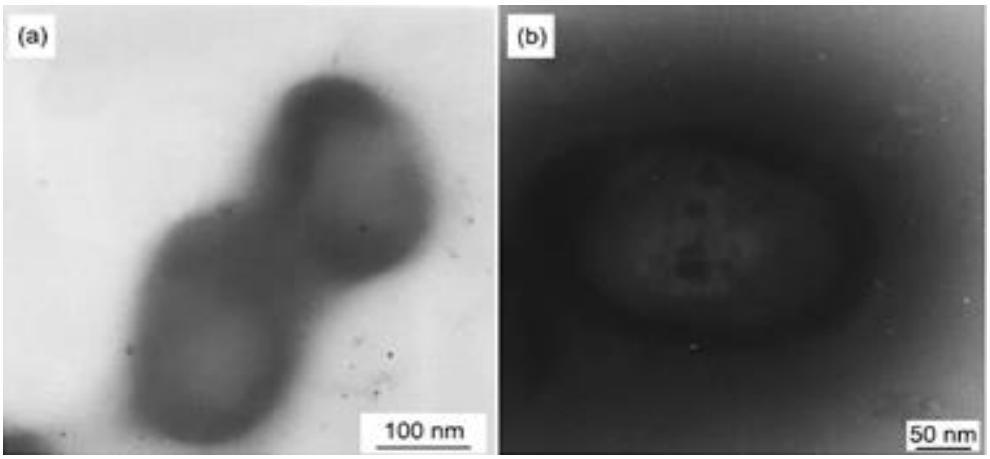

Figure 2.4. TEM micrograph: (a) interaction of silver nanoparticles with *E: coli*, (b) penetration of silver nanoparticles (Source: Raffi et al. 2008)

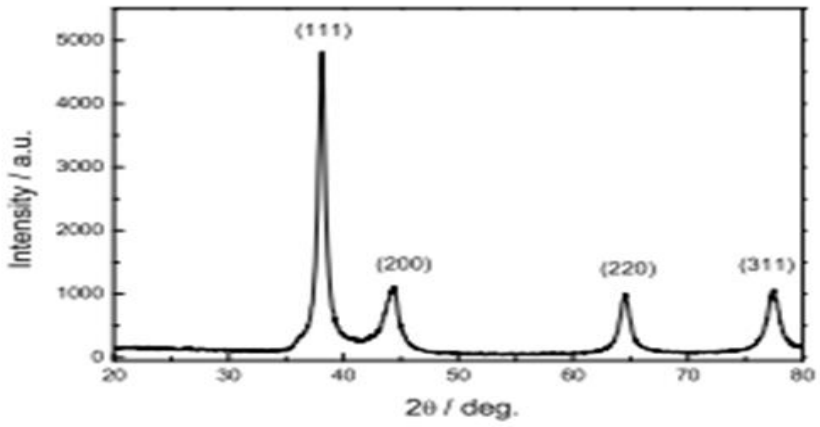

Figure 2.5. XRD pattern of silver nanoparticles synthesized by inert gas condensation process (Source: Raffi et al. 2008)

Kim et al. also studied about the antimicrobial activity of Ag nanoparticles against *Escherichia coli*, and *Staphylococcus aureus*. They supply various concentrations of Ag nanoparticles in liquid systems and they used Muller Hinton agar plates for tests. The free-radical generation effect of Ag nanoparticles on microbial growth inhibition was investigated by electron spin resonance spectroscopy and

minimum inhibitory concentration (MIC) which is the lowest concentration of an antibacterial agent to inhibit the visible growth of a microorganism after overnight incubation. was calculated. In their results, Ag nanoparticles were most effective against E. coli. The MIC of Ag nanoparticles against *E. coli* may be estimated between 3.3 nM and 6.6 nM. For *S. aureus*, Ag nanoparticles showed a mild growth-inhibitory effect even in high concentration. MIC of Ag nanoparticles against S. aureus was estimated to be more than 33 nM. The results shows Ag nanoparticles are effective antimicrobial agent (Kim et al. 2007). MIC results and TEM image of Ag nanoparticles are shown in Table 2.1 and Figure 2.6, respectively.

Table 2.1. MIC results of Ag nanoparticles
(Source: Kim et al. 2007)

	MIC of Ag Nanoparticles
Yeast (ATCC19636)	>6.6 nM
E.coli (ATCC43890)	>3.3 nM
St. Aureus (Bovine Mastitis)	>3.3 nM

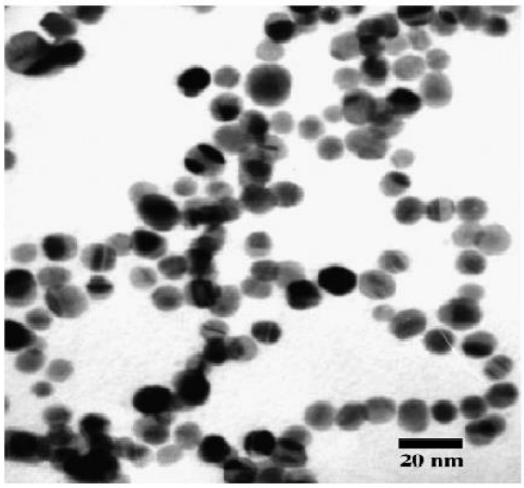

Figure 2.6. TEM image of Ag nanoparticles dispersed on a TEM copper grid
(Source: Kim et al. 2007)

Baheiraei et al. used sol–gel method to reach antibacterial activity of silver-doped silica thin films on glazed surface of ceramic tiles. They investigated the Ag/SiO_2 thin films with Fourier transform infrared spectroscopy (FTIR), scanning electron microscopy (SEM), X-ray diffraction (XRD) and wavelength dispersive spectrometry (WDS). According to XRD results, while SiO_2 was observed by peaks at 21.988^0,

28.48^0, 31.468^0, and 36.038^0, silver was shown with a broad peak at $2\theta = 38.118^0$, 44.278^0 and 64.278^0. Determination of the silver ion concentration being released from Ag/SiO_2 films over a 24 day period was studied by atomic absorption spectroscopy (AAS). The presence of Ag elements on the surface of the coated tiles were observed and the results showed that coating films illustrated an perfect antibacterial performance against *Escherichia coli* and *Staphylococcus aureus* (Baheiraei, Moztarzadeh, and Hedayati 2012). XRD patterns of Ag/SiO2 silica gel heat treated at 1100 ^{0}C are shown in Figure 2.7.

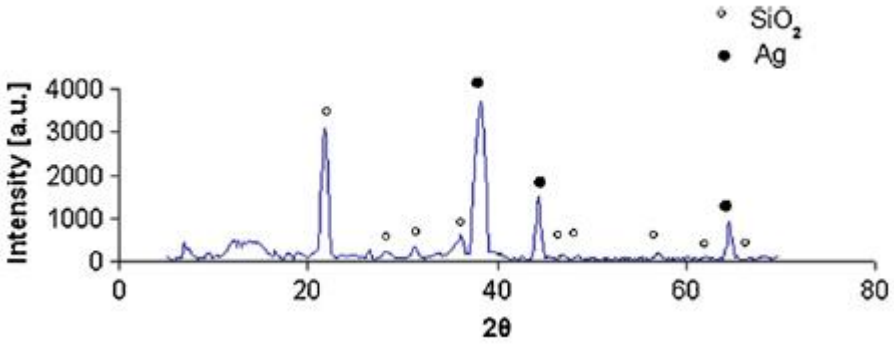

Figure 2.7. XRD patterns of Ag/SiO2 silica gel heat treated at 1100 ^{0}C
(Source: Baheiraei, Moztarzadeh, and Hedayati 2012)

Hilonga et al. investigated the anibacterial properties of silver-doped silica powder. They synthesized silica matrices with a sol-gel route which allows one to easily tailor textural and chemical properties. Pure silver nanoparticles (Ag^0), silver in ionic state (Ag^+), AgCl nanoparticles, and the mixture of Ag^0 and AgCl were obtained with this route. In the antibacterial activity tests, the powders containing Ag^0, Ag^+ and AgCl nanoparticles were compared with the pure silica (SiO_2). All silver-doped products showed large zone of inhibition than pure silica product (Hilonga et al. 2012). A schematically illusrated large zone of inhibition is shown in Figure 2.8.

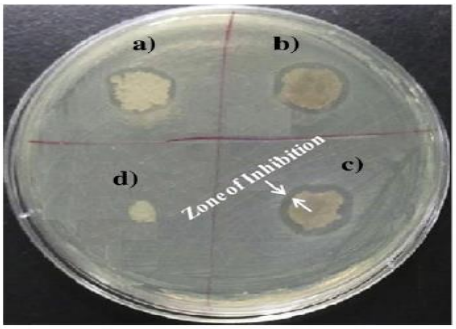

Figure 2.8. (a) AgCl nanoparticles, (b) pure silver nanoparticles (Ag^0)/Ag^+, (c) mixture of Ag^0 and AgCl, (d) un-doped (pure silica (SiO_2)) (Source: Hilonga et al. 2012)

Soo-Hwan et al. observed the antibacterial properties of silver nanoparticles by field emission scanning electron microscope (FE-SEM) with measuring the growth curves, formation of bactericidal reactive oxygen species (ROS), protein leakage, and lactate dehydrogenase activity involved in the respiratory chain. They used *Gram-positive Staphylococcus aureus* and *Gram-negative Escherichia coli* as a bacteria. They investigated the growth rates under varying concentrations of silver nanoparticles incubation times, incubation temperatures, and pHs. They observed that antibacterial properties of silver nanoparticles did not fluctuate with temperature or pH (Kim et al. 2011). FE-SEM micrograph of S. aureus (A, B) and E. coli (C, D). (A, C: control; B, D: treated with Ag-NPs) are shown in Figure 2.9.

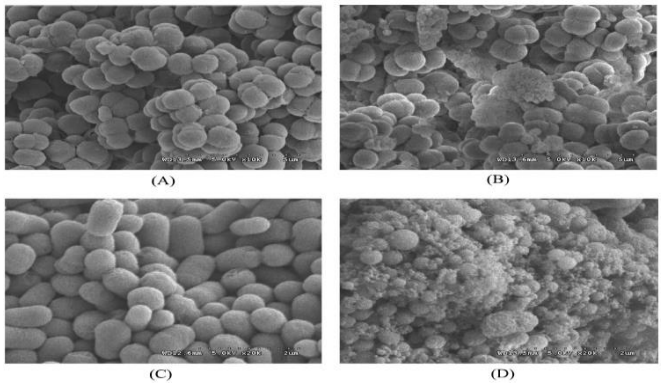

Figure 2.9. FE-SEM micrograph of *S. aureus* (A, B) and *E. coli* (C, D). (A, C: control; B, D: treated with Ag-NPs) (Source: Kim et al. 2011)

Titanium dioxide (TiO_2) is a nontoxic material and has been applied in environmental treatments such as water and air purification, water disinfection and sterilization because of its unique properties such as strong photocatalytic activity and chemical stability (Fujishima, Rao, and Tryk 2000). The TiO_2 photocatalysts have been

investigated extensively for the killing or growth inhibition of bacteria. TiO_2 particles catalyze the killing of bacteria on illumination by near-UV light. The generation of active free hydroxyl radicals (-OH) by photoexcited TiO_2 particles is probably responsible for the antibacterial activity. In recent years, nano TiO_2 has been paid more attention by many researchers.

Fu et al. used sol-gel chemistry approach to fabricate nanoparticles of TiO_2 in its anatase form. They prepared different percentages of vanadium-doped TiO_2 nanoparticles, which extended the TiO_2 absorption wavelength from the ultraviolet to the visible region. XRD, TEM, AFM, and UV-vis spectroscopy are used to charecterize the synthesized nanocomposites have a size of about 12-18 nm. The TiO_2 nanocomposite coatings have been applied on glass slide substrates. Two types of bacteria, *Escherichia coli* and *Bacillus megaterium* were used to investigate the antibacterial activity of TiO_2 nanocomposites (Fu, Vary, and Lin 2005). XRD pattern of TiO_2 nanoparticles prepared by the hydrolysis of titanium isopropoxide, and catalyzed by either HNO_3 or $HClO_4$ are shown in Figure 2.10.

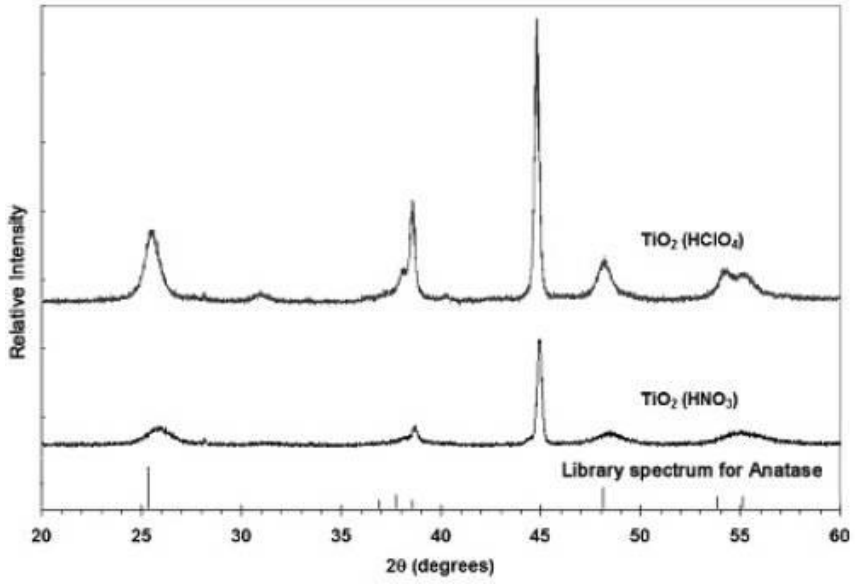

Figure 2.10. XRD pattern of TiO_2 nanoparticles prepared by the hydrolysis of titanium isopropoxide, and catalyzed by either HNO_3 or $HClO_4$. A library spectrum of anatase TiO_2 is marked for comparison
(Source: Fu, Vary, and Lin 2005)

Montazer et al. Prepare the silver loaded nano TiO_2 as a nanocomposite through UV irradiation in an ultrasonic bath to introduced an effective nanocomposite antimicrobial agent for wool fabric. To confirm the presence of existence of

nanocomposite on the fabric surface EDS spectrum, SEM images, and XRD patterns were used. Antibacterial activities of the treated fabrics improved when increasing the concentration of Ag/TiO_2 nanocomposite (Montazer et al. 2011).

Xue et.al. synthesized Boron-doped TiO_2 (B/TiO_2) nano-materials with a sol-gel method and characterized with Xray diffraction pattern (XRD), transmission electron microscopy (TEM), X-ray photoelectron spectroscopy (XPS), Fourier transform infrared spectrum (FT-IR) and UV‐vis diffuse reflectance spectra (DRS). They investigated the the antibacterial properties of B/TiO_2 nano-materials on *Escherichia coli* with the test of bacterial inhibition zone. The results of antibacterial experiment under visible light irradiation show that B/TiO_2 nano-materials exhibit enhanced antibacterial efficiency compared with non-doped TiO_2 (Xue, Wang, and Yang 2013). XRD patterns of pure TiO2-500 ˚C and B/TiO_2 calcined at different temperatures are shown in Figure 2.11.

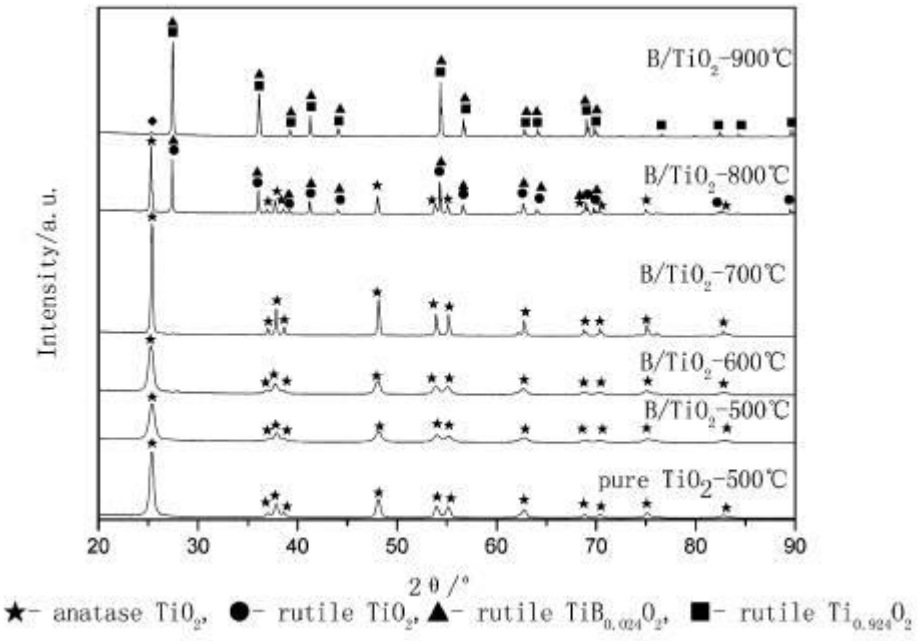

Figure 2.11. XRD patterns of pure TiO2-500 ˚C and B/TiO_2 calcined at different temperatures (Source: Xue, Wang, and Yang 2013)

Amin et al. prepared TiO_2–Ag nanocomposite with the sol–gel method and use and an azeotropic distillation with benzene for dehydration of the gel. TEM micrographs and XRD patterns showed that spherical nanosized Ag particles (≈10 nm) were deposited among TiO_2 particles. They studied the antibacterial activity of calcined

powder at 300 and 500 °C in the presence and in the absence of UV irradiation against *Escherichia coli* (Amin, Pazouki, and Hosseinnia 2009).

Zhang et al. studied about copper element whivh was added in pure titanium by a powder metallurgy to produce a new antibacterial titanium– copper alloy (Ti–Cu alloy). The phase constitution was analyzed by XRD and the microstructure was observed under SEM equipped with EDS. They used two method to understandt antibacterial property of the Ti–Cu alloy which were agar diffusion assay and plate-count method. In agar diffusion assay No antibacterial activity was detected however plate-count results indicated that the Ti–Cu alloy exhibited strong antibacterial property (Zhang et al. 2013). Typical photos of colonization by *E. coli* and *S. aureus* at 24 h are shown in Figure 2.12.

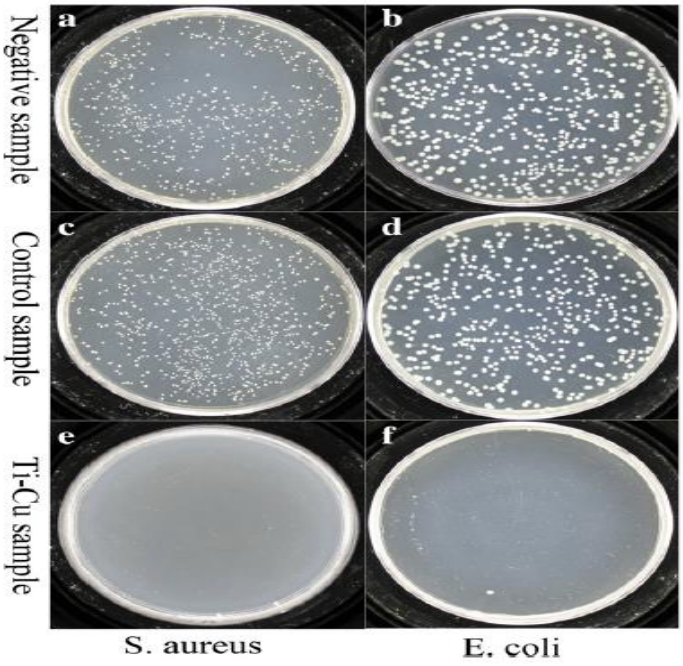

Figure 2.12. Typical photos of colonization by *E. coli* and *S. aureus* at 24 h. (a)–(b) negative sample, (c)–(d) control sample and (e)–(f) Ti–Cu sample
Source: (Zhang et al. 2013)

Zinc oxide (ZnO) have received increasing attention in recent years, because they are not only stable under harsh processing conditions, but also because they are generally regarded as safe materials to human beings and animals. The nanoparticles have selective toxicity to bacteria but exhibit minimal effects on human cells (Xie et al. 2011). Scanning electron microscopic images are shown in Figure 2.13.

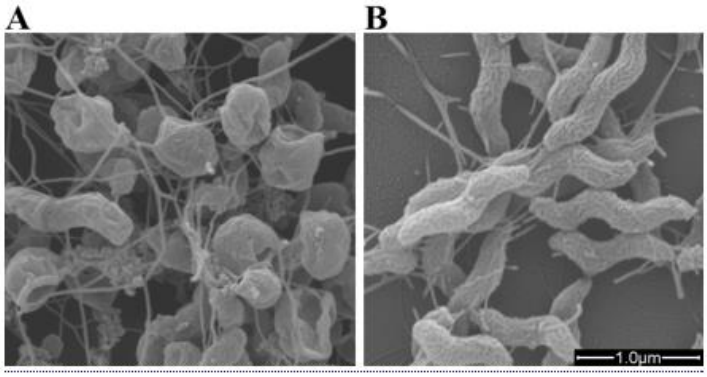

Figure 2.13. Scanning electron microscopic images of *C. Jejuni* (A) *C. jejuni* cells in the mid-log phase of growth were treated with 0.5 mg/ml of ZnO nanoparticles for 12 h under microaerobic conditions (B) Untreated cells from the same growth conditions were used as a control
(Source: Xie et al. 2011)

Among the various metal oxides studied for their antibacterial activity, zinc oxide nanoparticles have been found to be highly toxic. Moreover, their stability under harsh processing conditions and relatively low toxicity combined with the potent antimicrobial properties favours their application as antimicrobials. Zinc oxide nano particles have selective toxicity to bacteria and only exhibit minimal effect on human cells (Ravishankar Rai and Jamuna Bai 2011).

Li investigated a precipitation method to prepare nanoscale zinc oxide (ZnO) as the precursor of silver coated antibacterial nanocomposite. He prepared silver loadeded zinc oxide nanocomposites by using hydrolysis method. He compared The average diameters and morphology of ZnO nanocomposites before and after silver loaded. He coated silver on the precursor succesfully and increase the diameter of ZnO nanocomposites slightly. The results showed that with average diameter of of 170 nm zinc oxide powder presented good dispersibility and uniform size (Li 2012). Size distribution and XRD patterns of ZnO and Ag/ZnO are shown in Figure 2.14 and Figure 2.15, respectively.

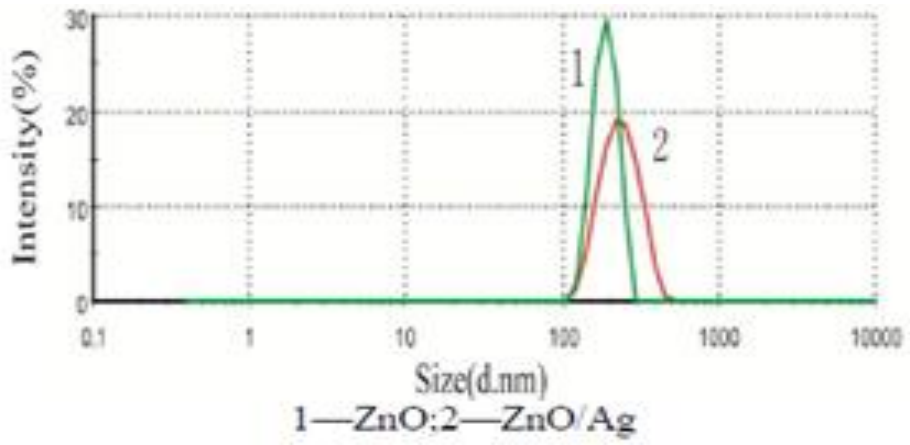

Figure 2.14. Size distribution of ZnO and Ag/ZnO
(Source: Li 2012)

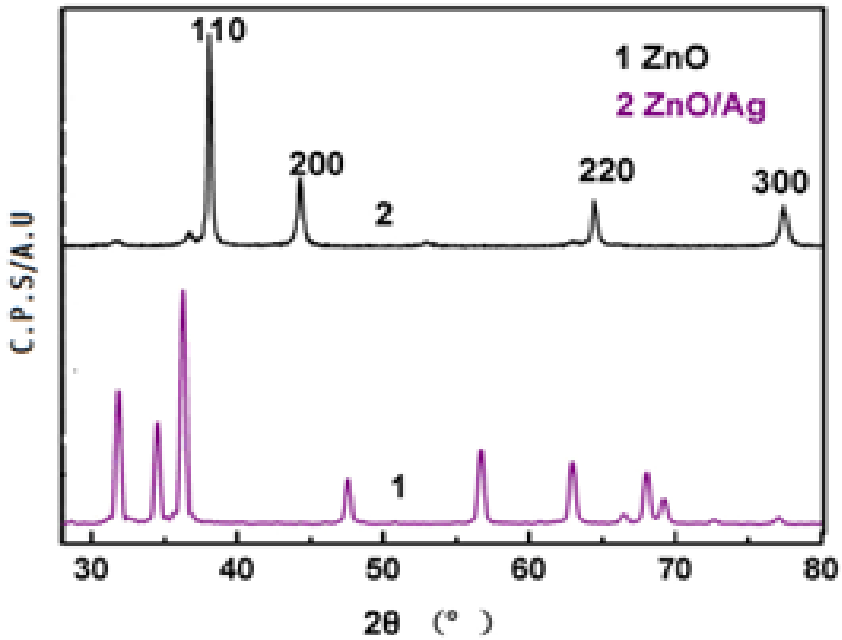

Figure 2.15. XRD patterns of ZnO nanoparticles before and after silver loaded
(Source: Li 2012)

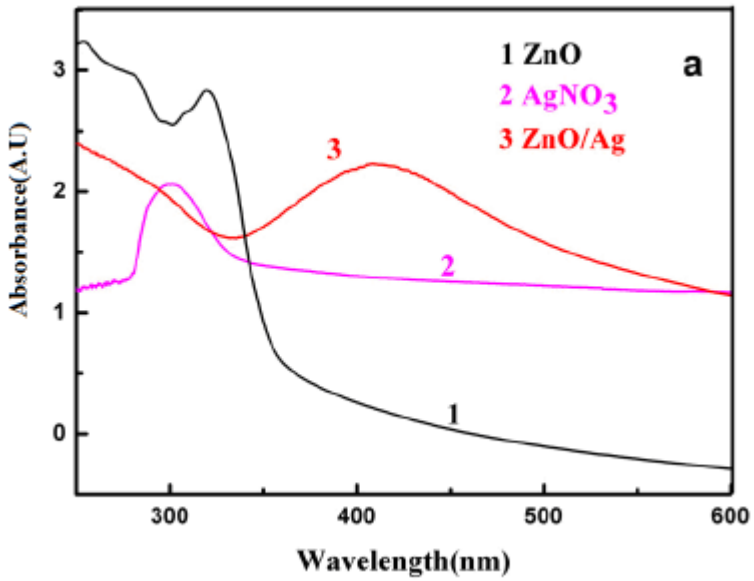

Figure 2.16. UV-vis spectra of ZnO, AgNO3 and Ag/ZnO solutions
(Source: Li 2012)

Liu et al. investigated antibacterial activities of zinc oxide nanoparticles and their mode of action against an important foodborne pathogen, which is *Escherichia coli*. They used zinc oxide nanoparticles with sizes of 70 nm and concentrations of 0, 3, 6 and 12 mmol l^{-1}. They achieved complete inhibition of microbial growth at the concentration level of 12 mmol l^{-1} or higher. They used Scanning electron microscopy (SEM), transmission electron microscopy (TEM), and Raman spectroscopy to characterize the changes of morphology and cellular compositions of bacterial cells treated with zinc oxide nanoparticles. The results demonstrated that zinc oxide nanoparticles have antibacterial activity against *E. Coli* so zinc oxide nanoparticles could potentially be used as an effective antibacterial agent to protect agricultural and food safety (Liu et al. 2009). Transmission electron microscopic image of zinc oxide nanoparticle suspension are shown in Figure 2.17.

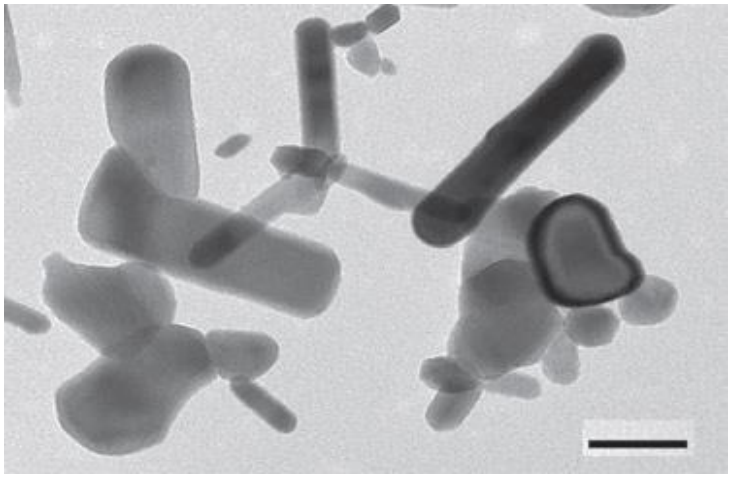

Figure 2.17. Transmission electron microscopic image of zinc oxide nanoparticle suspension (Source: Liu et al. 2009)

Magnesium oxide (MgO) which is a lightweight inorganic antibacterial agent has attracted intensive interests because of the advantages of large raw materials, lower cost, simple antibacterial conditions and safe materials to human beings. Therefore there are many studies in literature. Rao et al. synthesized MgO nanopowders doped with different ions (Li^{+}, Zn^{2+} and Ti^{4+}). X-ray diffraction (XRD), transmission electron microscope (TEM) and X-ray photoelectron spectroscopy (XPS) analysis were used to characterize the structures and morphologies of the as-obtained precursors and nanopowders. They investigated the influence of three metal ions doping on the antibacterial properties of MgO nanopowders against *Escherichia coli*. The results showed that the influence of different ions doping on the antibacterial properties of MgO mainly lies on oxygen vacancies and basicity of nanopowders (Rao et al. 2013).

Lellouche et al. described a novel water-based synthesis of magnesium fluoride nanoparticles. They showed the antimicrobial activity was dependent on the size of the nanoparticles. They coated glass surfaces and demonstrated inhibition of bacterial colonization for 7 days by using the sonochemical process. Also, the antimicrobial activity of MgF_2 nanoparticles against established biofilms was examined (Lellouche et al. 2012).

Ren et al. investigated the Antibacterial behaviors of magnesium (Mg) based metal, pure Mg and AZ31 alloy, with and without surface coatings. The results show that, with a mild increase of the pH value, pure Mg with porous silicon-contained (Si) coating by micro-arc oxidation still maintained its antibacterial ability, however pure Mg and AZ31 alloy with fluorine-contained (F) and Si coatings by chemical conversion

lost their antibacterial abilities with nearly no change of the pH values, because of the much dense coatings on surfaces (Ren et al. 2011).

CHAPTER 3

POLYMER-MATRIX COMPOSITES

A composite material is a material system is made up of two or more macro constituents that differ in shape and chemical composition and which are insoluble in each other. The aim of a composite material is to achieve a combination of properties that is not displayed by any single material, and also to incorporate the best characteristics of each of the component materials (Callister and Rethwisch 2012). Composite materials are becoming an essential part of todays materials because of the advantages such as low weight, corrosion resistance, high fatigue strength and faster assembly. They are extensively used as materials in making aircraft structures, electronic packaging to medical equipment, and space vehicle to home building (Shaw et al. 2010).

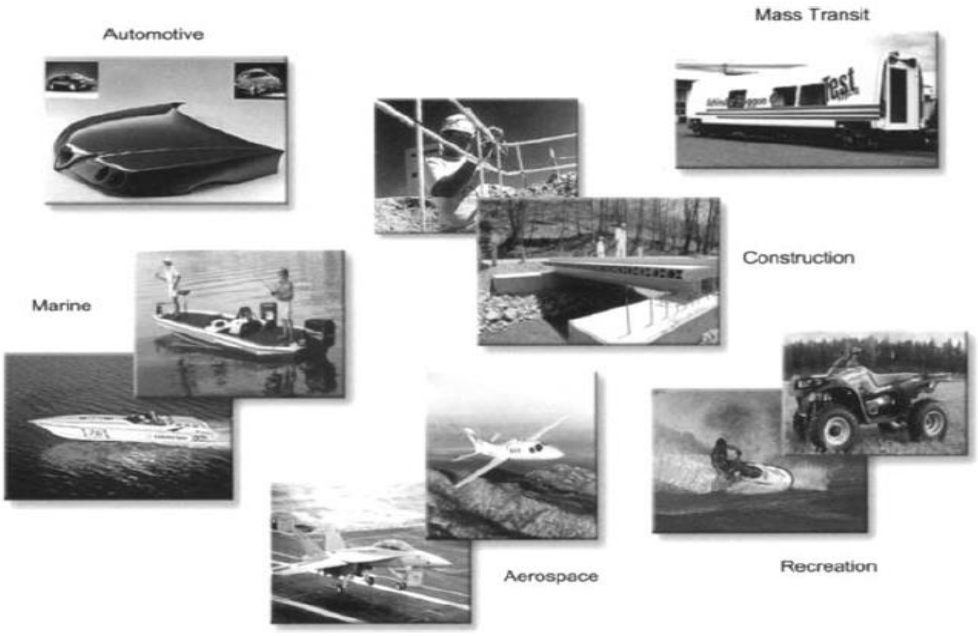

Figure 3.1. Composite applications are varied and expanding
(Source: Campbell Jr 2003)

There are three major points to be included in a definition of an acceptable composite material:

- They are generally consist of two or more physically distinct and mechanically separable materials.
- They are produced by mixing the different materials in order to achieve controlled and uniform dispersion of the constituents.
- They have superior mechanical properties and in some cases, they show uniquely different properties from their constituent (Mayer, Wang, and Neitzel 1998).

Types of composite materials may be divided into three general categories:

- Fibrous composites which consist of fibers in a matrix.
- Laminated composites which consist of layers of various materials.
- Particulate composites which are composed of particles in a matrix (Chandramohan and Marimuthu 2011).

According to the matrix phase, composites can be classified as metal matrix composites (MMCs), ceramic matrix composites (CMCs), and polymer matrix composites (PMCs) (Avila et al. 2003).

Polymer Matrix Composites (PMCs) are the most common composites which are discussed here and known as particulate reinforced polymers. In these materials, a polymer-based resin is used as a matrix, and E-glass, carbon and aramid can be used as the reinforcement materials. Metal Matrix Composites (MMCs) are generally used in the automotive industry, these materials use a metal such as aluminium as the matrix, and reinforce it with fibres such as silicon carbide. Ceramic Matrix Composites (CMCs) use a ceramic as the matrix and reinforce it with short fibres, or whiskers such as those made from silicon carbide and boron nitride (Chandramohan and Marimuthu 2011).

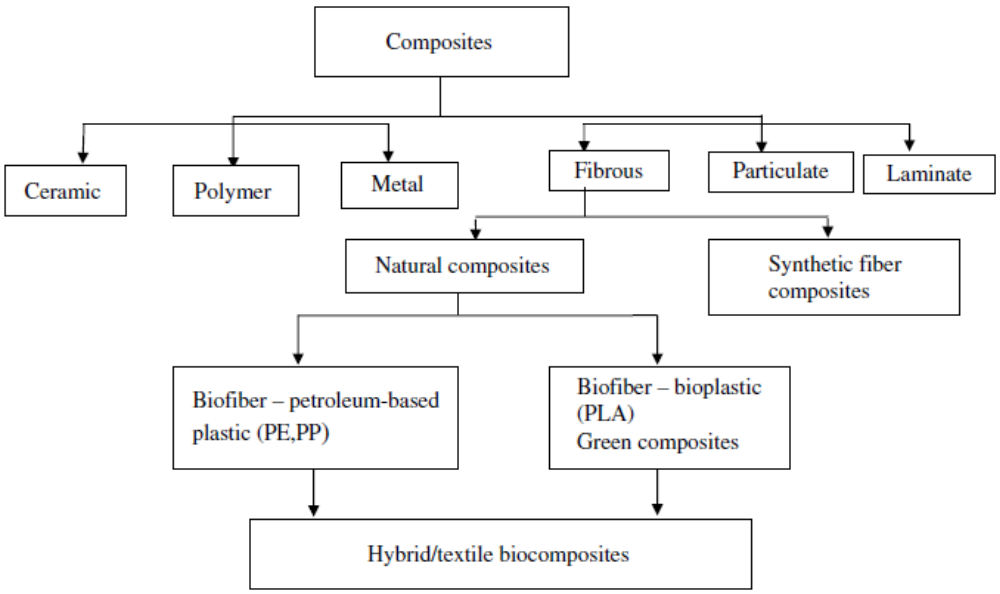

Figure 3.2. Classification of composites
(Source: Malhotra et al. 2012)

To produce a proper composite system, matrix selection plays very critical role. Because fibers' proper position are controlled by matrix, and matrix protects the fibers from abrasion. Matrix distributes the load between fibers equally and also provides interlaminar shear strength. A matrix which choosen properly also provides resistance to heat, chemicals and moisture. The another important properties are that, it cures at as low a temperature as possible and yet has a long pot or out-time life and is not toxic. Table 3.1 shows the most prevalent thermoset resins which are used for composite matrices. Thermosets or thermoplastics are types of matrices for polymeric composites. Thermoset resins usually consist of a resin (e.g. epoxy, polyester) and a compatible curing agent. When the curing agent and resin are initially mixed, a low-viscosity liquid are formed which cures as a result of either internally generated (exothermic) or externally applied heat. As a result of the curing reaction, a series of cross-links are formed between the molecular chains therefore one large molecular network is formed that can not be reversible. However in thermoplastics, cross-links between the molecular chain are not formed. On heating to a high enough temperature, they either soften or melt, so they can be reprocessed a number of times.

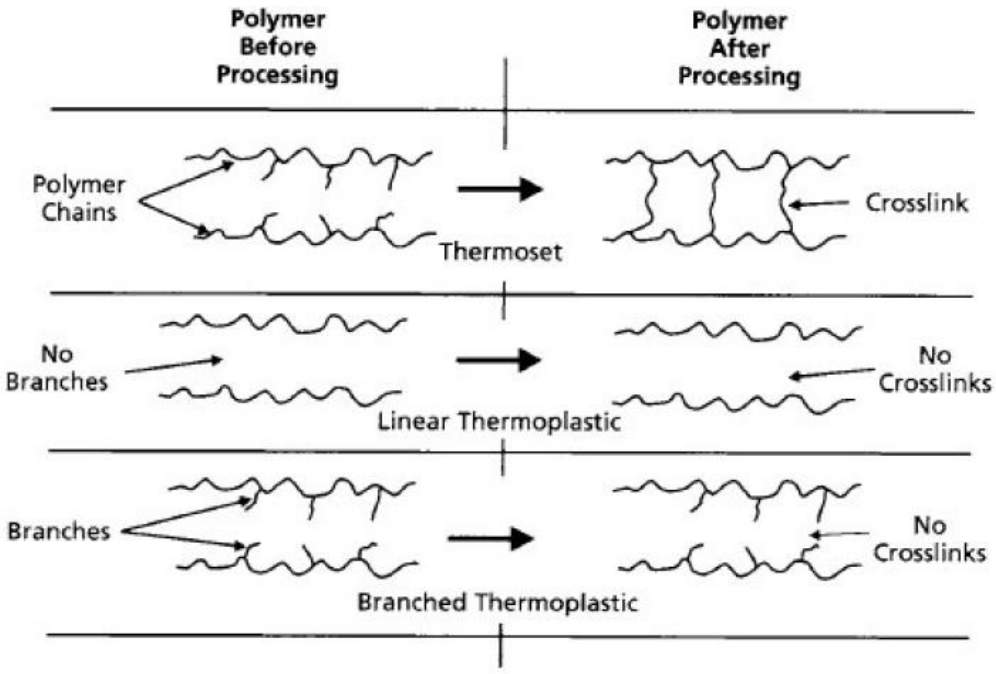

Figure 3.3. Comparison of Thermoset and Thermoplastic Polymer Structures
Source: (Campbell Jr 2003)

The second important component of the composite is the fibers. The primary role of the fibers is to provide strength and stiffness. There are continuous or discontinuous fibers embedded in a matrix in advanced composites. Common fibers include glass, aramid and carbon.

Glass fiber-based products are very important for industry because they are environmentally friendly(Bender and Hadley 1994). Glass is an amorphous material consisting of a silica (SiO_2) backbone with various oxide components to give specific compositions and properties. Glass fibers consist of high amount silicon oxide, aluminum oxide, boron oxide, calcium oxide, magnesium oxide and sodium oxide. Glass fibers are made from different formulations. 'E' (electrical) being the most common all-purpose glass while 'S' (high strength) is made for special applications. Quartz fiber products are the purest form of silica. The chemical composition of these glass formulations is shown Table 3.1.

Table 3.1. The chemical composition of glass formulations
(Source: Hull et al. 1996)

wt%	E glass	C glass	S glass
SiO_2	52.4	64.4	64.4
Al_2O_3, Fe_2O_3	14.4	4.1	25.0
CaO	17.2	13.4	--
MgO	4.6	3.3	10.3
Na_2O, K_2O	0.8	9.6	0.3
Ba_2O_3	10.6	4.7	--
BaO	--	0.9	--

E-glass which is the most common and least expensive provide a good combination of tensile strength (500 ksi) and modulus (11.0 msi). S-2 glass having a tensile strength of 650 ksi and a modulus of 12.6 msi is more expensive, however is 40% stronger than E-glass. Quartz fiber is a quite expensive, ultra-pure silica glass with a low dielectric fiber and is used primarily in demanding electrical applications and semi-conductor manufacturing (Campbell Jr 2003). Other types that available commercially are C-glass (Corrosion) which used in chemical environments, such as storage tanks. The another type is R-glass and used in structural applications such as construction. Also D-glass is (Dielectric) used for applications which requires low dielectric constants, such as radomes; and A-glass (Appearance) used to improve surface appearance. Some combinational types such as E-CR glass (Electrical and Corrosion resistance) and AR glass (Alkali Resistant) also exist (Mallick 2007).

Aramid fiber (e.g. Kevlar) is an extremely tough organic fiber with low density and exhibits excellent damage tolerance. Although it has a high tensile strength, it performs poorly under compression. It is also sensitive to ultraviolet light and its use should be limited to long-term service at temperatures less than 350 ^{0}F.

Carbon fibers have the best combination of strength and stiffness properties with strengths ranging from 300 to 1000 ksi and moduli ranging from 30 to 145 msi but are also more expensive than the others. It has a low density with excellent radar transparency and a low dielectric constant. Due to its low density, it exhibits very high specific strength and modulus at room temperature. However, being a polyethylene its use is limited to within 290 ^{0}F. Like aramid, Spectra has excellent impact resistance; however, poor adhesion to the matrix is a problem, although plasma treatments can be employed to improve the adhesion (Campbell Jr 2003).

Table 3.2. Comparison of most commonly used resin systems
(Source: (Campbell Jr 2003)

Polyesters	Used extensively in commercial applications. Relatively inexpensive with processing flexibility. Used for continuous and discontinuous composites.
Vinyl Esters	Similar to polyesters but are tougher and have better moisture resistance.
Epoxies	High performance matrix systems for primarily continuous fiber composites. Can be used at temperatures up to 250-275F. Better high temperature performance than polyesters and vinyl esters.
Bismaleimides	High temperature resin matrices for use in the temperature range of 275-350F with epoxy-like processing. Requires elevated temperature post cure.
Polyimides	Very high temperature resin systems for use at 550-600F. Very difficult to process.
Phenolics	High temperature resin systems with good smoke and fire resistance. Used extensively for aircraft interiors. Can be difficult to process.

Besides, each of the resin systems has its some advantages and disadvantages. The use of a particular resin system depends on the application. These considerations involve mechanical strength, cost, smoke emission, temperature excursions, resistance to corrosion etc (Mazumdar 2001). A summary of most commonly used resin systems can be found in Table 3.2.

Table 3.3. Properties of typical high strength fibers
(Source: Campbell Jr 2003)

Fiber	*Density lb/in³*	*Tensile Strength (ksi)*	*Elastic Modulus (msi)*	*Strain to Failure (%)*	*Diameter (Mils)*	*Thermal Expansion Coefficient 10-6 in/in/ F*
E-glass	0.090	500	11.0	4.8	0.36	2.8
S-glass	0.092	650	12.6	5.6	0.36	1.3
Quartz	0.079	490	10.0	5.0	0.35	1.0
Aramid (Kelvar 49)	0.052	550	19.0	2.8	0.47	–1.1
Spectra 1000	0.035	450	25.0	0.7	1.00	–1.0
Carbon (AS4)	0.065	530	33.0	1.5	0.32	–0.2
Carbon (IM-7)	0.064	730	41.0	1.8	0.20	–0.2
Graphite (P-100)	0.078	350	107	0.3	0.43	–0.3
Boron	0.093	520	58.0	0.9	4.00	2.5

Table 3.3 shows the physical and mechanical properties of some of the commercially important fibers which are glass, organic, pan based carbon, pitch based carbon. Most common fiber reinforcements are glass, carbon, graphite and aramid.

Each type of fiber reinforcement has its own advantages over other and used for suitable applications (Long 2005).

In the present study, polyester was used as the matrix material while quartz particles used as reinforced and filler materials. Polyester-quartz systems have attracted considerable attention in recent years because of their high specific strength and stiffness, high fracture resistance, good impact, abrasion, fatigue and corrosion resistance and low cost (Malhotra, Goda, and Sreekala 2012).

CHAPTER 4

EXPERIMENTAL

4.1. Materials

Quartz particles and polyester (Polylite ® 442-020 unsaturated polyester) were used to manufacture thermoset based composite material. Unsaturated polyester which is produced by copolymerization of styrene and polyester was obtained from AKG Yalıtım ve İnşaat Malzemeleri San. ve Tic. A.Ş. Unsaturated polyester was used as a polymer matrix. Quartz having three different particle sizes over 100 microns was used as reinforcing material, In addition to quartz particles having 45 micron used as a filler.

To fabricate composite stone, polyester resin and quartz particles are blended in the ratio of 10 to 90% respectively. The resin contains three additional compounds; the first one is 3-methacryloxypropyltrimethoxysilane (in content of 1wt%) used as adhesion promoter, surface modifier for polymer synthesis and crosslinker. Cobalt(II) 2-ethylhexanoate (in content of 0,2wt%) is used as accelerator and tert-butyl peroxybenzoate (in the content of 2wt%) is used as catalyst. These constituents are blended with the resin for production of composite stones by applying combined vacuum, vibration and pressing processes which are named as vibropress, simultaneously. Upon fabrication of the stones, they are subjected to surface preparation and polishing processes. The blend formulations were developed in collaboration with AKG Yalıtım ve İnşaat Malzemeleri Sanayi ve Ticaret A.Ş.

To prepare polyester samples with antibacterial properties, a number of different antibacterial agents in various fractions were added into the polyester resin. Based on these experiments, the proper antibacterial agents and their ratios were selected to fabricate composite stone. Finally, composite stones having best antibacterial influence on microorganisms were developed.

To obtain antibacterial effect, various materials such as silver, zinc oxide, titanium dioxide, magnesium oxide and calcium oxide were used in the form of powder.

The properties of the nanoparticles used with in the study are given in Table 4.3. In addition to those powders, synthesis of silver doped zinc oxide powder was performed. Silver nitrate ($AgNO_3$) in the form powder was purchaced from Merck Inc. and used as a silver source. The silver doped zinc oxide powder was also incorporated to the stone formulations according to procedure mentioned in the following sections. Properties of materials used to prepare polyester resin are shown in Table 4.1.

Table 4.1. Properties of materials used in the preparation of neat polyester resin

Materials / **Properties**	**Polylite 442-02-CT (Matrices)**	**Cobalt(II) 2-ethylhexanoate (Accelerator)**	**TBPB (Catalyst)**	**3-Methacryloxypropyltrimethoxysilane**
Viscosity (mPa.s) @20^{0}C	500-600	16	4	2.8
Density (g/cm^3) @20^{0}C	1.08-1.12	0.963	1.03	1.04
Refractive index n (20,D),	-	-	-	1.432
Boiling point (^{0}C) @(1.3 hPa)	-	-	-	85
Flash point (^{0}C)	-	-	55	110
Melting point (^{0}C)	-	-	0	

Table 4.2. Formulation of the materials used in composite stone fabricate with/without antibacterial additives

Properties / Materials	Weight %	Density (g/cm ^{3})
Quartz (Reinforcement Materials 0.1/0.4 mm)	24.4	2.65
Quartz (Reinforcement Materials 0.3/0.7 mm)	23.4	2.65
Quartz (Reinforcement Materials 0.7/1.2 mm)	14.7	2.65
45micron quartz (Filler)	27.6	2.65
Polylite 442-02-CT (Matrices)	9.9	1.08-1.12
Silane	1 wt % of polyester	1.04
Tert-butyl peroxybenzoate (TBPB) (Catalyst)	2 wt % of polyester	1.03
Cobalt(II) 2-ethylhexanoate (Accelerator)	0.2 wt % of polyester	0.963
Antibacterial Agent	5 wt % of polyester	-
Ti(IV)O_2 (Pigment)	8.1 wt % of polyester	-

Formulations of the materials used in composite stone fabricate with/without antibacterial additives are given in Table 4.2.

Table 4.3. Features of the antibacterial agents used in the preparation of antibacterial nanocomposites

Antibacterial Agent / Properties	Ag	ZnO	$Ti(IV)O_2$	MgO	CaO
BET Surface Area (m^2/g)	-	-	35	-	-
Average Particle Size (nm)	115	322	296	190	175
True Density (g/cm^3)	10.42	-	3.9	-	-
Purity (%)	99.99	99	99.5	-	-

Properties of the antibacterial agents used in the preparation of antibacterial nanocomposites are shown in Table 4.3.

4.1.1.Preparation of Silver Doped ZnO by Impregnation Method

Various chemical synthesis methods for Ag doped ZnO have been employed by several researchers and it was found that the morphology and size of the particles are greatly affected by the reaction condition; including temperature, pH, reactant concentration, reactant ratio, calcination temperature, drying method.

In this study, Ag-doped ZnO (Ag/ZnO) powders were prepared by impregnation methods.

Firstly, 20g of ZnO and 5g of water were mixed for half an hour. After adding 1wt% of $AgNO_3$, this mixture was stirred continuously for 4 hours at 4-5 pH and 70 ^{0}C. Upon stirring, an aqueous solution containing zinc nitrate and silver oxide was obtained. Nitrate ions were filtered and washed with distilled water for purification. After then, the sample was heated at 140 ^{0}C for 2h. This is the evoporation step to remove oxygene gases. The remaining Ag/ZnO collected in filter paper was dryed at 400 ^{0}C for 3 hours

in an oven and Ag/ZnO powders were obtained and shown in Figure 4.3. The stage of composite stone fabrication, the synthesized Ag/ZnO powders were added to the polyester system based on the procedure are shown in Figure 4.2.

Figure 4.1. Antibacterial agents used with the study a) Silver powder b) Zinc oxide powder

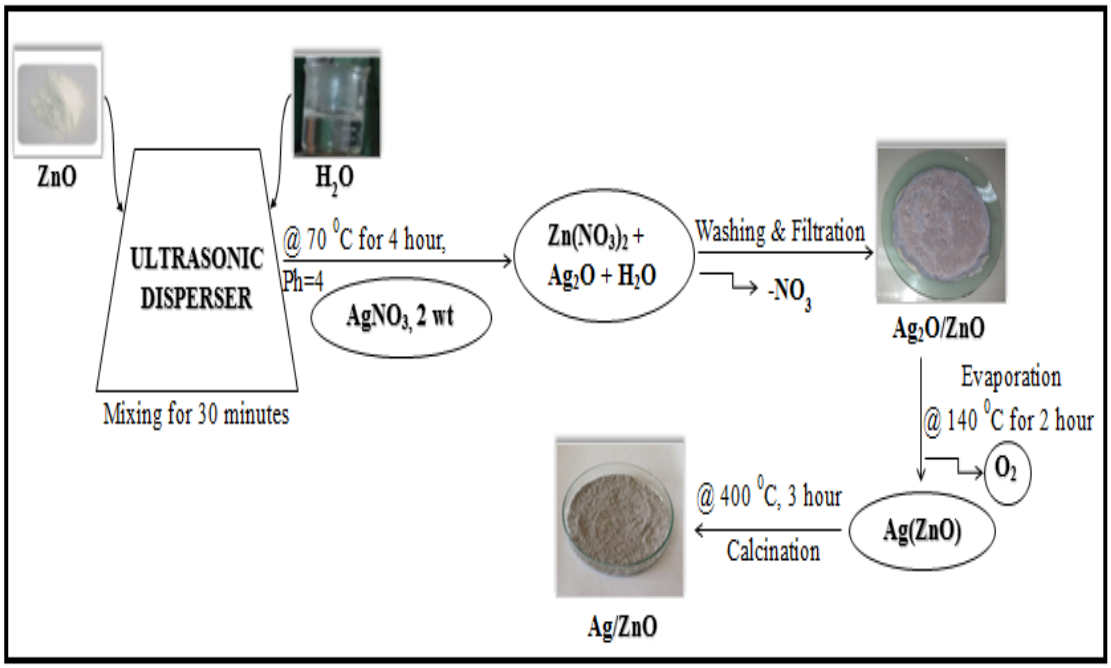

Figure 4.2. Schematic illustration of synthesis of Ag/ZnO powder by impregnation method

Figure 4.3. Synthesized Ag/ZnO powders by impregnation methods

4.1.2. Polyester – Quartz Composite Stone Preparation

Polyester is a long-chain polymer which chemically composed of an ester, a dihydric alcohol and a terephthalic acid, formed by the esterification condensation of polyfunctional alcohols and acids. Unsaturated polyesters refer to that family of thermosetting polyesters with alkyl resins as the backbone. They are mostly used with reinforced materials in various industries. Several studies of quartz as filler in composites materials were carried out to improve the strength, to reduce the production cost, to adjust the viscosity and to make smooth surface (Yoshida et al. 2002).

In this study, quartz with three different molecular size were used as a reinforcement materials in matrices and purchased from AKG Yalıtım ve İnşaat Malzemeleri Sanayi ve Ticaret A.Ş.

Stone that contains 90 wt.% SiO_2 and 10 wt.% polyester was used for antibacterial coating products. There are four main steps (casting, vibropress, surface preparetion and polishing process) for the synthesis of polymeric composite stone as shown in Figure 4.4.

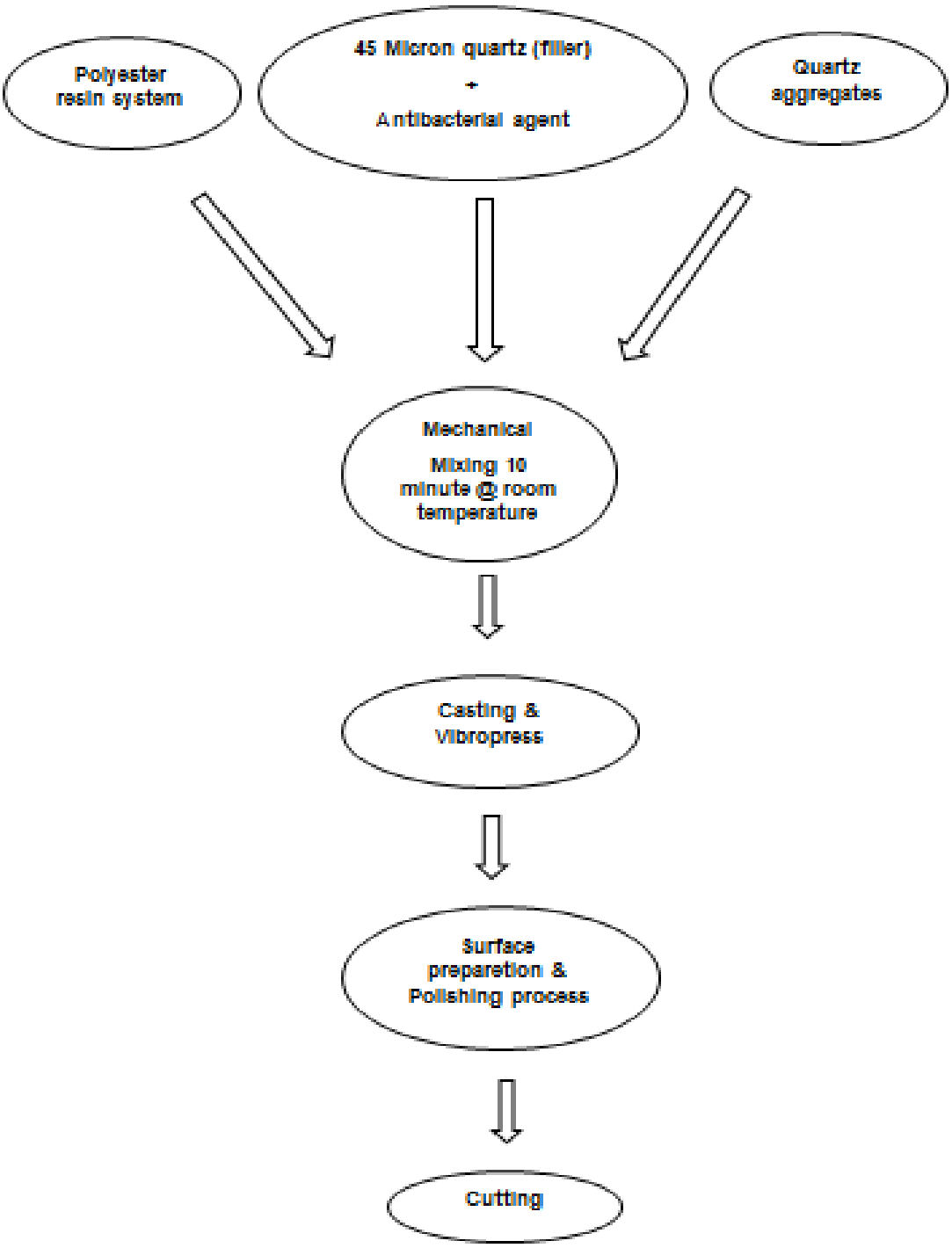

Figure 4.4. Processing stages of antibacterial polyester based nanocomposite stone

Schematic illustration of synthesized polymer based nanocomposite stone with antibacterial nanopowder is shown in Figure 4.5. At the beginning of the procedure, the accelerator was added into the polyester resin. Secondly, the catalyst was added to the system after ten minute. The reason of the ten minute delaying is to avoid explosion. Also in order to obtain smooth surface, silane was added. In the homogenization step,

quartz which have different size, and the prepared polyester resin were mixed by homogenizer mixer as shown in Figure 4.6. for 10 minutes. After this step, all ingredients were mixed homogenously. The another critical step was that, 45 microne quartz and antibacterial nanopowders were mixed because powders show a good dispersion within the 45 micron quartz. After then, this homogen mixture was added to the system and casting and vibropress process were applied as shown in Figure 4.7. Curing process was occured at 120 ^{0}C for half an hour. Finally these were subjected to surface preparetion and polishing process.

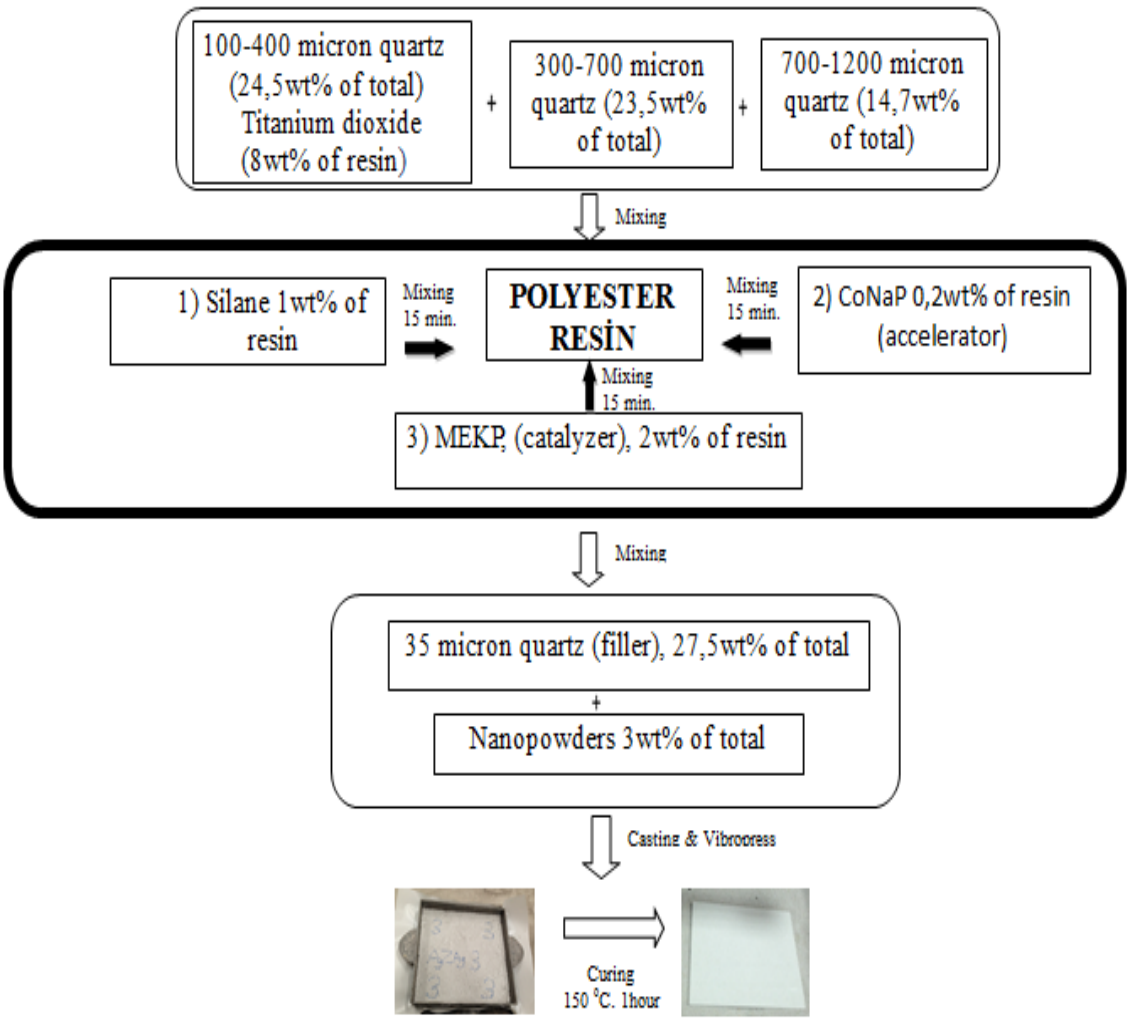

Figure 4.5. Schematic illustration of synthesized polymer based nanocomposite stone with antibacterial nanopowder

Figure 4.6. Homogenization of quartz nanoparticles and unsaturated polyester resin by homogenizer mixer

Figure 4.7. Vibropress machine used for polyester composite stone

Figure 4.8. Images of antibacterial composite stones after surface preparetion and polishing process

Figure 4.9. Images of antibacterial composite stones during cutting process

4.2. Characterization of Nanoparticles

4.2.1. Microstructural Features

4.2.2.1. X-Ray Diffraction (XRD)

In order to identify the crystallinity of particles, Phillips™ Xpert diffractometer were used with Cu Kα irradiation as a radiation source. Particles were scanned in the interval of a 2θ range from 2°-80° at 40 kV and 30 mA. XRD patterns were obtained.

4.2.2.2. Scanning Electron Microscopy (SEM)

The microstructures measurements of particles were performed by using a Phillips™ XL-30S FEG Scanning Electron Microscopy (SEM). The Backscattered Electrons Detector (BSED) was especially used to detect the silver element coated onto the zinc oxide surfaces. All the sample surfaces were gold-coated by a sputtering apparatus before SEM examination.

4.2.2.3. Dynamic Light Scattering (DLS)

The average particle size and size distribution based on number of silica nanoparticles were measured with Zetasizer 3000HS by using Dynamic Light Scattering (DLS) technique. The wavelength of the laser light employed in the instrument was 633 nm, which capable of detecting a minimal particle size of 2 nm. Measurements for each sample were repeated at least three times.

To analyze the particle size distributions, nanoparticles were dispersed in water and mixed for about 30 minutes until obtaining stable dispersion.

4.2.2.4. Fourier Transform Infrared Spectroscopy (FTIR)

Shimadzu FTIR 8201instrument was used to identify the molecular functional groups of polyester. The spectrum was collected in absorption mode from 400 to 4000 cm^{-1} at room temperature. KBr pellet technique was applied to record FTIR spectrum.

4.2.2.5. X-ray Photoelectron Spectroscopy (XPS) Technique

The oxidation state of Ag on the ZnO surface was analyzed by X-ray photoelectron spectroscopy.

4.2.2.6. Inductively Coupled Plasma Spectrometer (ICP)

Inductively Coupled Plasma Emission Spectroscopy, like atomic absorption methods, is a technique for determining the concentration of elements in solution. The advantage of ICP is its ability to analyze many elements, either simultaneously or in a rapid sequential manner depending upon the type of the instrument employed. The sample may be either liquid or solid, but solid materials must undergo a suitable preparation involving dissolution, decomposition, or extraction. ICP AES spectroscopy is based upon the principle that the energy of emission is specific for each element. The liquid sample is atomized by a nebulizer into a stream of argon gas, which carries the atomized sample into the plasma where the elements in solution are thermally excited. The excited elements emit photons, which are detected by one or more photomultiplier tubes, depending upon the type of instrument.

In the present study, ICP AES spectroscopy was used to determine whether the of Ag, ZnO, Ag/ZnO, MgO, CaO and TiO_2 particles moved to buffer solution from antibacterial polyester based nanocomposite stone by analyzing the liquid phase.

4.3. Characterization of Unsaturated Polyester Resin (UPR)

4.3.1. Rheological Properties

A TA Instruments AR2000ex oscillatory rheometer was used to analyze the rheological properties of unsaturated polyester resin (UPR). The rheological measurements of UPR were repeated three times and the average of the values were taken. TA Instruments AR2000ex oscillatory rheometer used within the experiments is shown in Figure 4.10.

Figure 4.10. TA Instruments AR2000ex oscillatory rheometer used within the experiments

4.3.2. Microstructural Features

4.3.2.1. Scanning Electron Microscopy (SEM)

Dispersion of the nanoparticles in the organic phase was identified by the help of scanning electron microscope (SEM) (Phillips™ XL-30S FEG). Before SEM analyses, polyester were applied for polishing. After that of all samples were gold-coated by a sputtering apparatus.

4.3.2.2. Fourier Transform Infrared Spectroscopy (FTIR)

In order to obtain information on the quality and the relative quantity of the inorganic phases, the Fourier Transform Infrared (FTIR) Spectroscopy was used. The IR Spectra of the composite were taken by placing the samples on the way of the beam using the transmission technique. Materials were analyzed by preparing KBr pellets. All spectra were taken between 400 cm^{-1} to 4400 cm^{-1} with a Shimadzu FTIR 8201 model instrument.

4.3.3. Thermal Properties

Thermal behavior of polymer composites is one of the most important factors for polymer processing and applications. Thermal analyses of the powder treated composites prepared by the two methods were conducted using Shimadzu Differential Scanning Calorimeter (DSC, 50), and Shimadzu Thermal Gravimetric Analyzer (TGA, 51). The experiments were carried out from room temperature up to 300 ^{o}C for the DSC analyses and up to 400 ^{o}C for the TGA analyses, at heating rates of 10 ^{o}C/min.

4.3.3.1. Differential Scanning Calorimeter (DSC)

Thermal behavior of composite was carried out by using differential scanning calorimeter, TA Instrument Q10. This analysis was performed by heating of 5.0 – 5.7 mg of sample from 50 to 300 °C with scanning rate of 20 °C/min in nitrogen gas atmosphere.

4.3.3.2. Thermogravimetric Analysis (TGA)

Investigation of thermal degradation response of the cured polyester nanocomposites and its nanocomposites containing 5 wt. % of antibacterial agents was done by the help of A Perkin Elmer, Thermal Gravimetric Analyzer (TGA). A sample of about 10 mg for each batch was placed into alumina crucible. The samples were then heated from ambient temperature up to 400 ^{o}C in a 50 ml/min nitrogen flow at 10 ^{o}C/min. Eventually, sample temperature, sample weight and its first derivative were

recorded as a function of time. In order to determine the weight percentage of powder in polyester samples, thermogravimetric analysis (TGA) was performed by using Perkin Elmer Diamond Thermogravimetric Analyzer.

4.4. Characterization of Composites Stone

4.4.1. Microstructural Features

4.4.2. Mechanical Property Characterization

4.3.2.1. Flexure Testing

Flexibility is the anothecritical feature for composites. Flexibility test was performed to determine the effect of powders addition on the composites flexibility by using Instron universal tensile testing machine model 2519-107. Figure for flexibility testing is shown in Figure 4.11. The samples were tested according to TS EN 14617-2 2008 standard. Tensile tests of the composites were carried at a ramp rate of 0.25 MPa/s and test was maintained until the force of 1200N was achieved. Each test was repeated two times and the mean values were used.

The images of neat composites before and after flexibility test are shown in Figure 4.12. a and b, respectively.

Flexural Strength, ASTM D 790M-86

$S=3PL/(2bd^2)$

S, Flexural strength, (Mpa)

P, Load applied at deformation point, (N)

L, Span length, (mm)

b, Sample thickness, (mm)

d, Sample width, (mm)

All specimens show linear stress-strain curves until failure. According to flexural stress vs. strain behaviour of the nanocomposites, Flexural strength of the nanocomposite increase with antibacterial particle content however, flexural strength of MgO stoneware decreases because of MgO particles is not suitabele for this system.

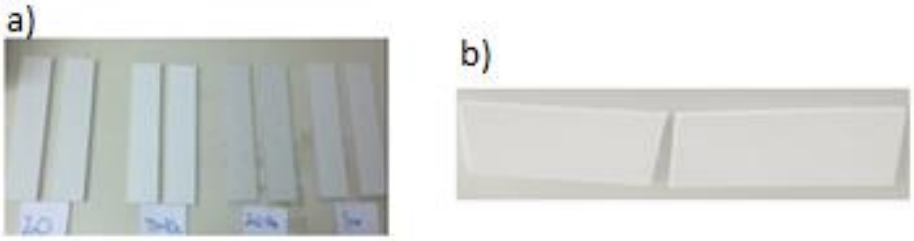

Figure 4.11. The images of neat composites before and after flexibility test

Figure 4.12. Photo of Instron universal tensile testing machine model 2519-107

4.3.2.2. Impact Resistance

The characteristic of resistance to fracture under the sudden application of an exerted force is called impact resistance. Impact testing on neat composites and composites with antibacterial agent were conducted using 1 kg steel ball in accordance with standart. These impact tests were preformed in AKG Yalıtım ve İnşaat Malzemeleri Sanayi ve Ticaret A.Ş. Schematic illustration of composites (a,b) before and (c) after impact test are shown in Figure 4.13.

Figure 4.13. Images of composites (a,b) before and (c) after impact test

Impact test was applied onto the neat composites and antibacterial powder loaded composites by using 1 kg steel ball according to standard. The composite used in the impact test is seen in Figure 4.14.

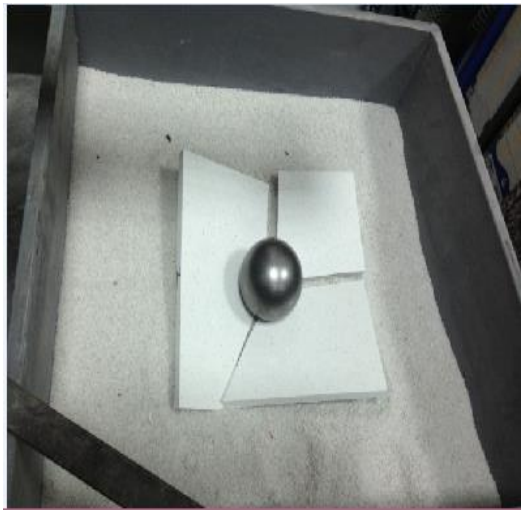

Figure 4.14. Fracture of neat composite under the sudden application of an exerted force

4.3.2.3. Scanning Electron Microscopy (SEM)

The microstructural characterization of neat stone and stone with antibacterial agent surfaces were performed by the help of scanning electron microscope (SEM) (Phillips™ XL-30S FEG). SEM analysis of polyester composite stones were helpful to investigate the dispersion level of powders within the composites. Before the analysis,

sample surfaces were grinded after that these were gold-coated in order to obtain electrically conductive surfaces to prevent charging.

4.5.Antibacterial Activity Tests

Polyester based nanocomposites treated with antibacterial powders (Ag, ZnO, Ag/ZnO, Ti(IV)O_2, MgO_2 and CaO) were tested for their antibacterial activity against *Escherichia coli* and *Bacillus subtilis* by the colony-count method. Initially, Antibacterial properties of the polyester resin containing antibacterial agents in different ratios were analysed. The amount of antibacterial agents to be incorporated into polyester based nanocomposite stones were determined after initial antibacterial tests. The equipment and media used for this purpose are LB, and LB agar.

4.5.1. Preparation of Media and Solutions

Luria Broth broth and Luria Broth agar were prepared. The broth and agar were dissolved in deionized water and distilled water in separate flasks by mixing with a magnet on magnetic stirrer. PH of the medium was adjusted to 7.3-7.4 with 1M NaOH. Media were autoclaved at 121 ^{0}C for 15 minutes. Luria Broth (LB) agar was cooled to 45-50 ^{0}C and 25 ml of medium were poured into sterile petri plates with a sterile 25 ml volumetric flask. After cooling, plates were stored at + 4 ^{0}C, and Luria Broth was stored at + 4 ^{0}C. Phosphate-Buffered Saline (PBS), pH 7.4 was prepared by dissolving 0.34 g KH_2PO_4, 1.58 g K_2HPO_4 and 8.0 g NaCl in 1 liter of distilled or deionized water. PH was adjusted to 7.4 and autoclaved at 121 ^{0}C for 15 minutes and stored at + 4 ^{0}C. Images of LB agar which spreaded on bacterial solution is shown in Figure 4.15.

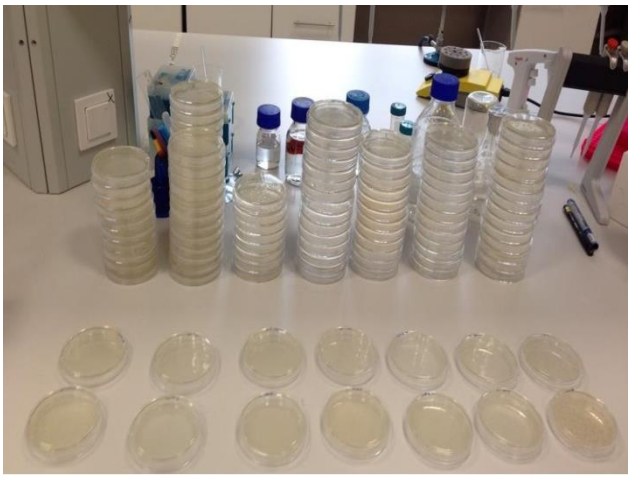

Figure 4.15. Images of LB agar which spreaded on bacterial solution

4.5.2. Broth Dilution Method

Bacteria from frozen glycerol stock at 20^0C were grown by streaking on a Luria Broth agar plate and incubated at 37^0C for overnight. The next day, a single colony was picked up with a cotton swap and the colony was added to 4 ml of sterile dH_2O. Test samples were placed into the tubes and all tubes were labeled. Medium and test samples were mixed by vortexing slowly. The tubes were incubated overnight at 37^0C with shaking at 180 rpm. Next day, the tubes were mixed again by vortexing. Serial dilutions of the bacterial solution up to 10^{-8} were prepared by tranferring 10 µl of the bacterial solution into 990 µl sterile PBS in eppendorf tubes. 100 µl from each dilution was taken and spread on LB agar plates in dublicates using glass spreaders. After incubating the plates at 37^oC overnight, the number of colonies in each plate were counted.

The activity is calculated with counting viable bacterial cells known as colony forming unit (cfu). Firstly, antibacterial property of cured polyester resin with these antibacterial agents is examined and applied stone by colony-count method. The highest antibacterial reduction was observed with silver and calcium oxide containing stone and polyester based nanocomposites.

Reduction and cfu/ml amount can be calculated using the formula.

cfu/ml= (numbert of colonies x dilution factor) / volume of culture plate

Reduction ratio %= $(X_o-X_r) \times 100 / X_o$

X_o= Bacteria/ml of control group after 24h

X_r= Bacteria/ml of test speciment after 24h

CHAPTER 5

RESULTS AND DISCUSSIONS

In this chapter, antibacterial effects of polyester based nanocomposite stone embedded with zinc oxide, silver, titanium dioxide, magnesium oxide, calcium oxide and silver dopeed zinc oxide were analyzed, which will be used in different applications, individually and combining them. The effects of various parameters such as the amount of antibacterial agents, and the preparation techniques for were investigated.

Rheological, thermal and microstructural features of both the stones and polyester based nanocomposites were also determined. In addition, mechanical properties (flexibility and impact features) of prepared stone and, polyester based nanocomposite were also determinde and their antibacterial property was tested.

5.4. Characterization of Nanoparticles

5.4.1. Microstructural Features

5.1.1.1. X-Ray Diffraction (XRD)

In Figure 5.1, x-ray diffractograms of nanoparticles (Ag, ZnO, Ag-doped ZnO) are shown. In this figure, it can be shown XRD patterns of nanoparticles exhibited sharp peaks. The Ag nanoparticles show four sharp peaks at $2\theta = 38.1^0$, 44.09^0, 64.36^0 and 77.29^0 corresponds to (111), (200), (220) and (311) planes of nanosilver, respectively (Khan et al. 2011). Therefore, the peak suggesting that the silver nanoparticles used in the study is highly crystalline structure. The diffraction did not suggest the presence of

possible impurities. The X-ray diffraction of the Ag nanoparticles suggested that silver existed purely in the face-centered cubic (fcc) structure.

The crystal structure of ZnO particles' peaks at 2θ = 31.67°, 34.31°, 36.14°, 47.40°, 56.52°, 62.73°, 66.28°, 67.91°, 69.03°, and 72.48° indicating that the samples were polycrystalline wurtzite structure. In addition, the XRD pattern of Ag/ZnO particles are shown in Figure 5.1. The X-ray diffraction of the Ag doped ZnO powder synthesized using the $AgNO_3$ suggested that silver existed purely in the facecentered cubic (fcc) structure. The diffraction did not suggest the presence of possible impurities, such as Ag_2O and $AgNO_3$.

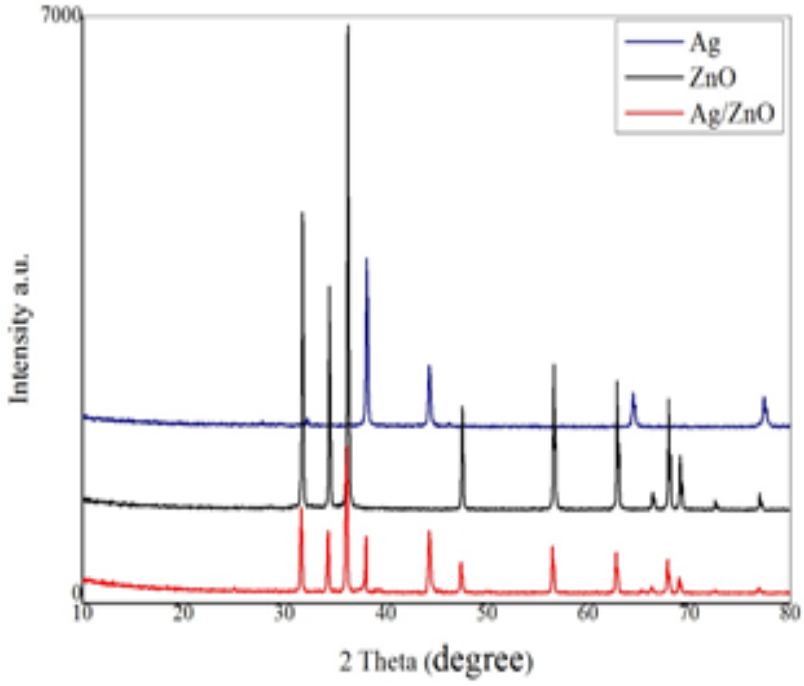

Figure 5.1. XRD pattern of Ag, ZnO, Ag/ZnO nanoparticles

5.1.1.2. Scanning Electron Microscopy (SEM)

SEM images of nanoparticles at high magnifications are given at below. The SEM images shown that nanoparticles have irregular shapes and some aggregates.

Ag NPs has certain spherical shapes and their average size was measured to be around 100 nm as shown in Figure 5.2. ZnO NPs has polycrystalline shapes and their average size was measured to be around 300 nm as shown in Figure 5.3. Ag/ZnO NPs

has irregular shapes and some aggregates and their average size was measured to be around 290 nm as shown in Figure 5.4. CaO NPs has irregular shapes and some aggregates and their average size was measured to be around 290 nm as shown in Figure 5.5. MgO NPs has irregular shapes and some aggregates and their average size was measured to be around 300 nm as shown in Figure 5.6. Ti(IV)O_2 NPs has irregular shapes and some aggregates and their average size was measured to be around 250 nm as shown in Figure 5.7.

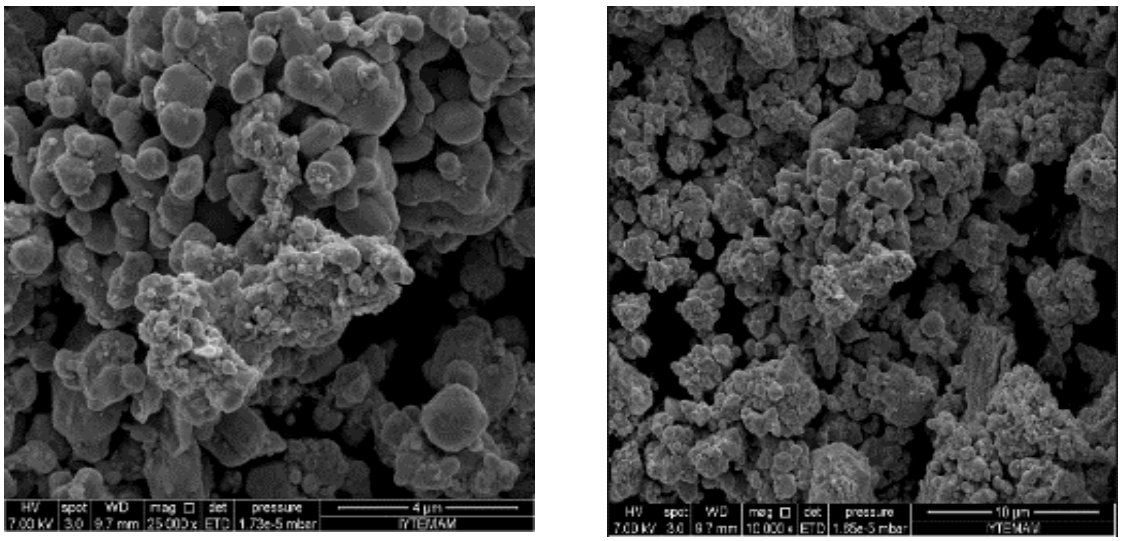

Figure 5.2.SEM images of a) Ag NPs (25000 x), b) Ag NPs (10000 x)

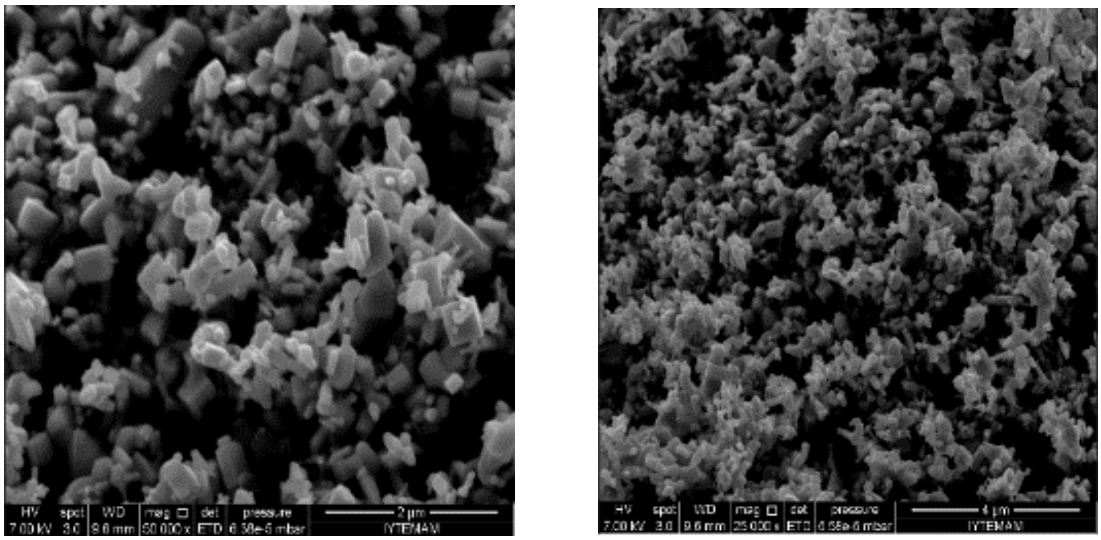

Figure 5.3. SEM images of a) ZnO NPs (50000 x), b) ZnO NPs (25000 x)

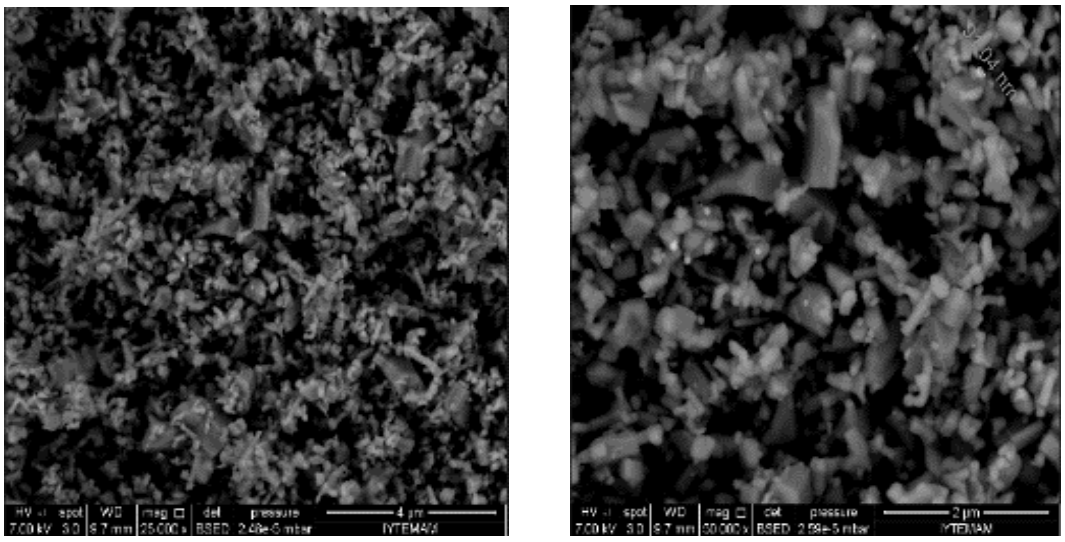

Figure 5.4. BSED images of a) Ag/ZnO NPs (25000 x), b) Ag/ZnO NPs (50000 x)

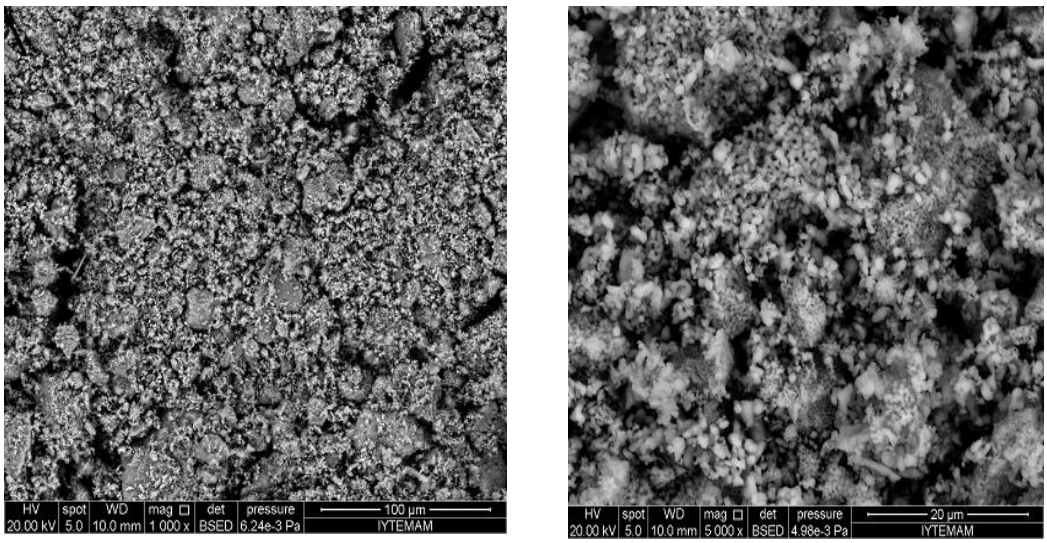

Figure 5.5. BSED images of a) CaO NPs (1000 x), b) CaO NPs (5000 x)

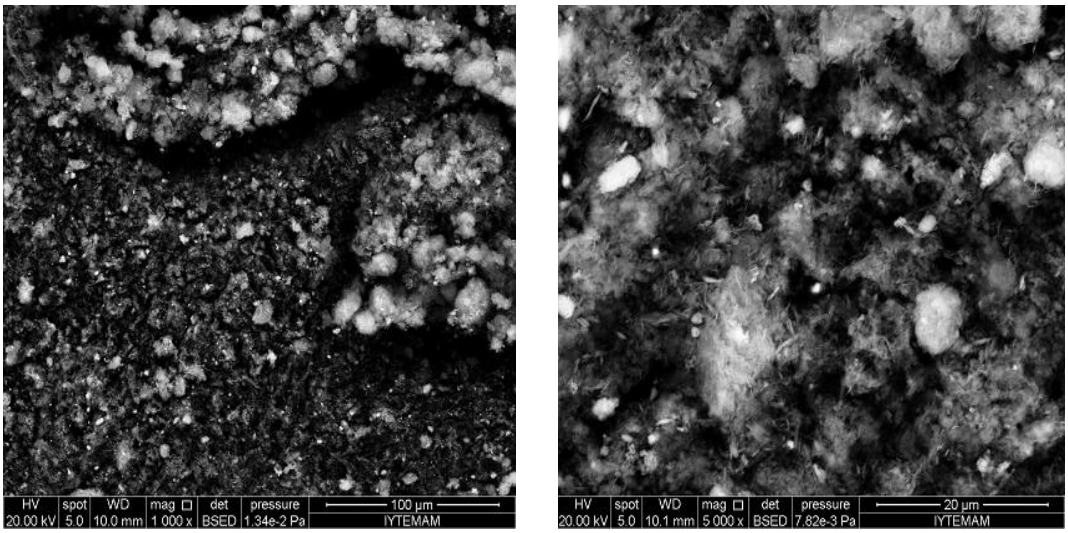

Figure 5.6. BSED images of a) MgO NPs (1000 x), MgO NPs (5000 x)

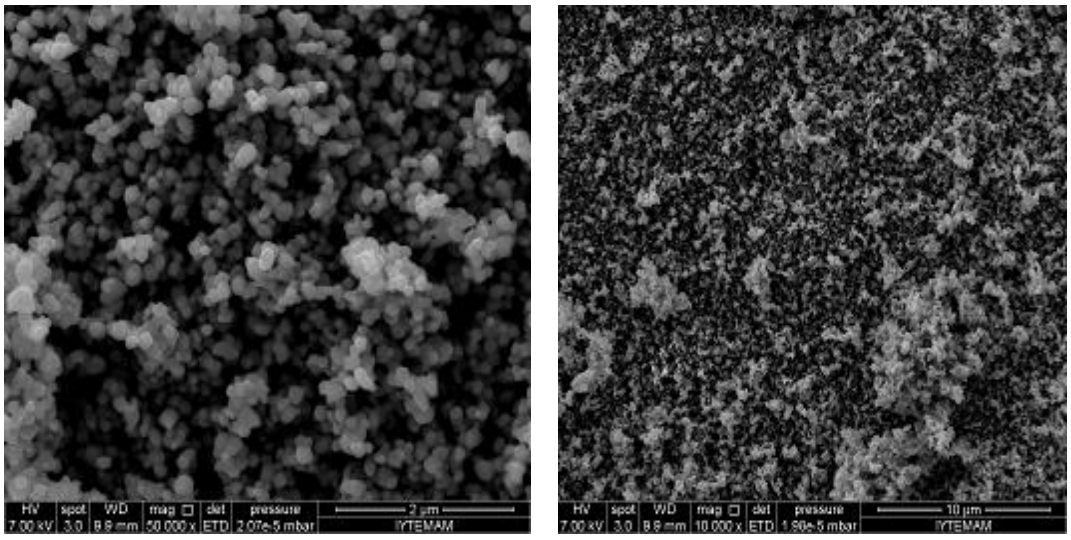

Figure 5.7. ETD images of a) Ti(IV)O_2 NPs (50000 x), Ti(IV)O_2 NPs (10000 x)

5.1.1.3.Dynamic Light Scattering (DLS)

Particulate size of nanoparticles were determined with dynamic light scattering (DLS) analyze by using malvern mastersizer 2000 instrument. Nano silver, zincoxide, and silver doped zincoxide particles has narrow diameter distrubition and average particle diameters, which are shown in Figure 5.8, 5.9 and 5.10, are around 115nm, 322nm and 296nm, respectively. The volume % and particle size distributions of other oxide nanoparticles are shown in Figure 5.11, 5.12 and 5.13 . Particle sizes of the particles were found as between 190-340 nm.

Average size of Ag, Ag/ZnO, ZnO, MgO, CaO, TiO_2 NPs were measured to be around 115, 296, 300, 190, 200, 210 nm as shown in Figs, respectively.

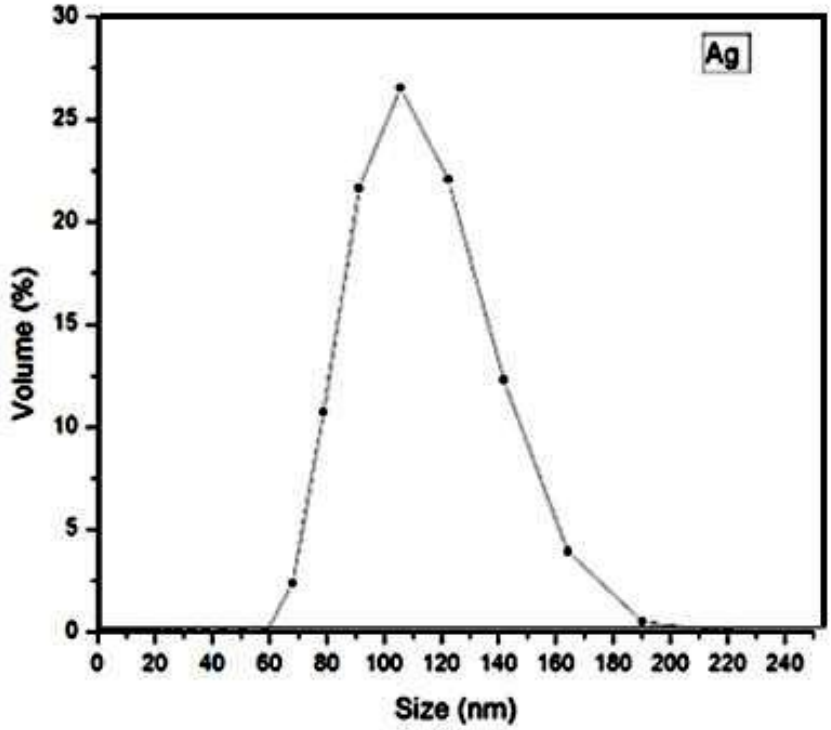

Figure 5.8 Size distributions of fumed Ag nanoparticles as a function of volume percentage

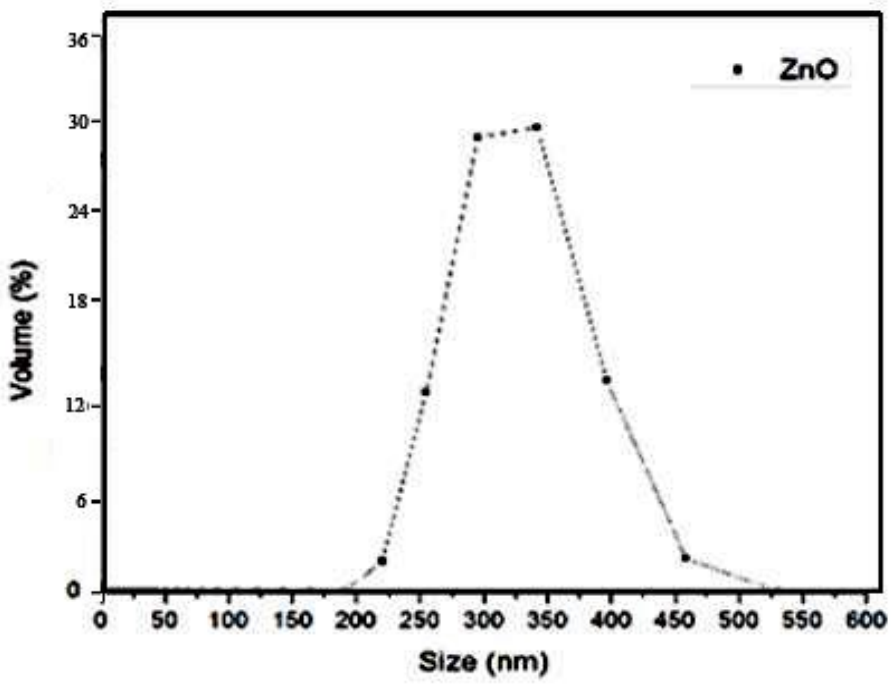

Figure 5.9. Size distributions of fumed ZnO nanoparticles as a function of volume percentage

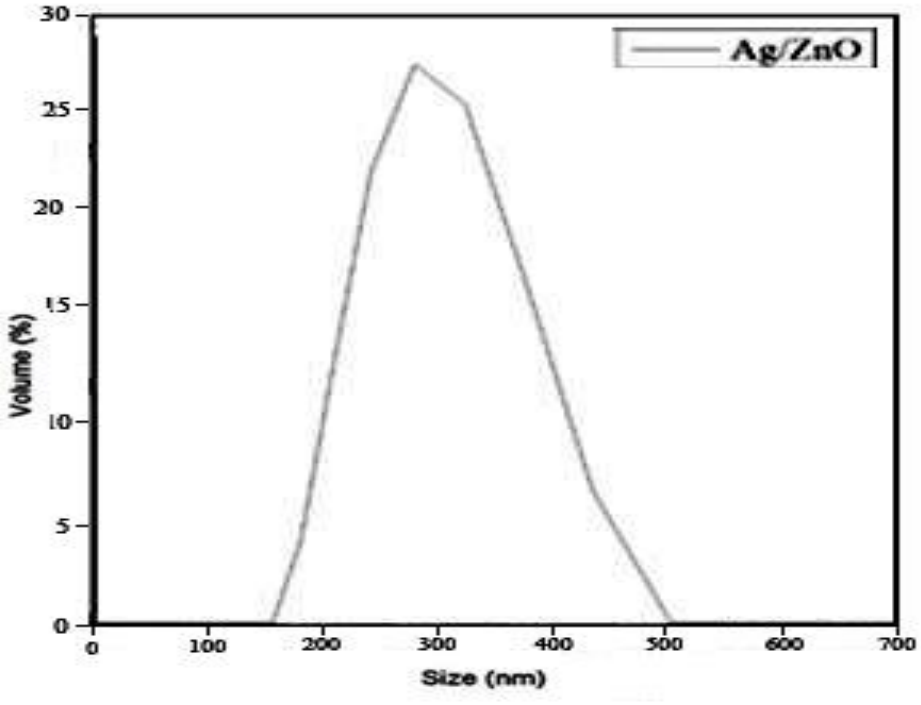

Figure 5.10. Size distributions of fumed Ag/ZnO nanoparticles as a function of volume percentage

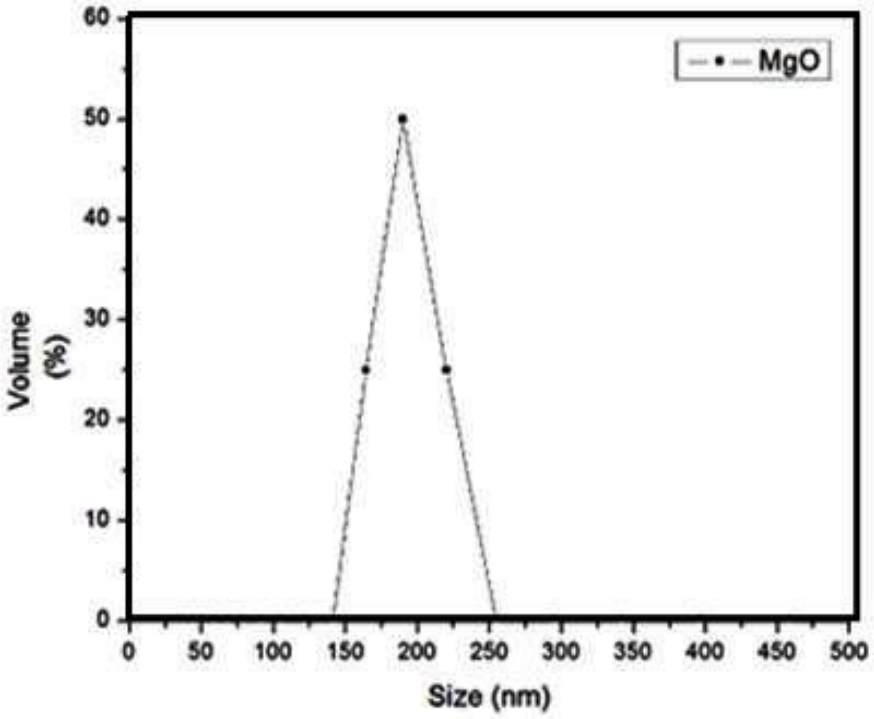

Figure 5.11. Size distributions of fumed magnesium oxide nanoparticles as a function of volume percentage

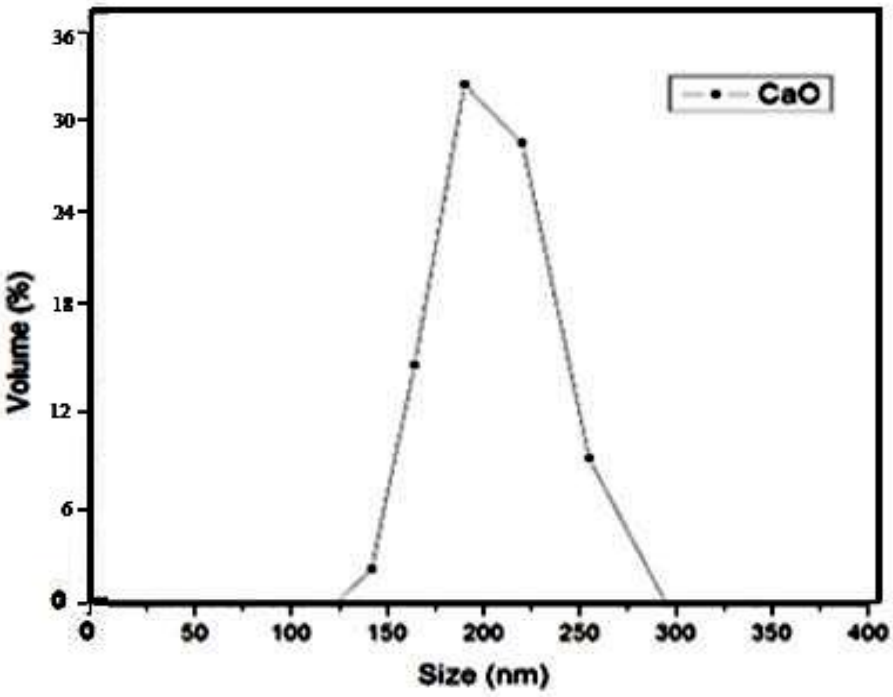

Figure 5.12. Size distributions of fumed calcium oxide nanoparticles as a function of volume percentage

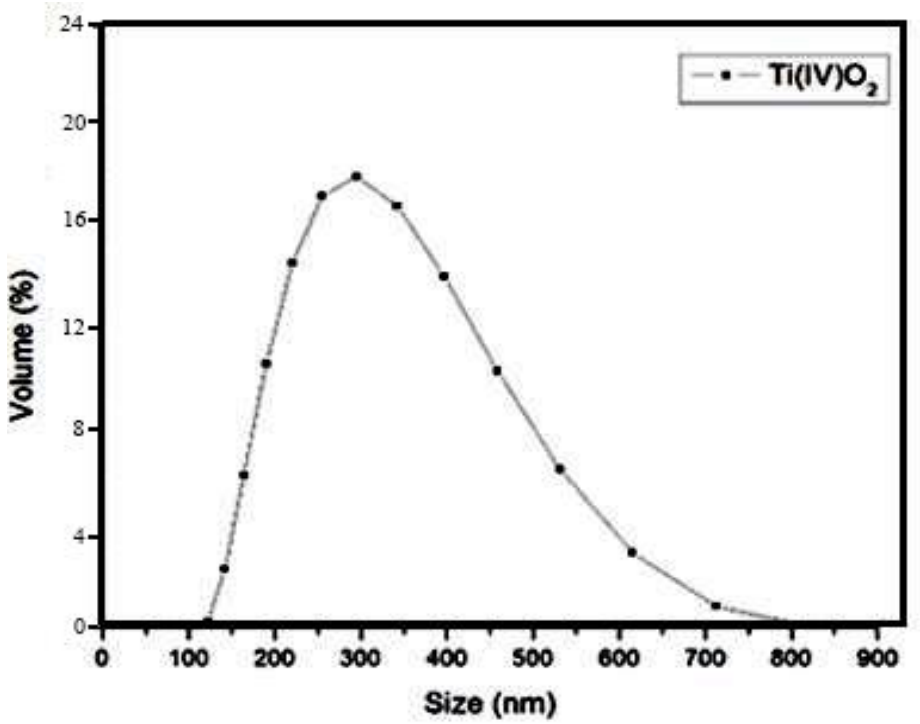

Figure 5.13. Size distributions of fumed TiO_2 nanoparticles as a function of volume percentage

5.1.1.4. X-ray Photoelectron Spectroscopy (XPS) Technique

The informative Zn, O, and Ag spectral sections of the survey analyses are presented by the accompanying high resolution regional spectra shown Figs. According to Figure 5.15, Zn (2p) signal splits into two symmetrical peaks as Zn (2p3/2) and Zn (2p1/2) due to strong spin orbit coupling. For pure ZnO nanoparticles, these peaks are located at 1021.41 and 1044.48 eV, respectively. Locations of these peaks slightly shift to higher BE values with Ag doping. Figure 5.14 indicates asymmetric O (1s) signals which can be divided into two symmetrical signals. For pure ZnO, the lower energy of O (1s) signal at 529.57 eV was attributed to lattice oxygen atoms and the high-energy portion of O (1s) signal located at 530.95 eV was associated with the chemisorbed oxygen, such as surface hydroxyl groups. Ag addition results in the positional shift in O (1s) spectra to higher BE values is shown in the Table 5.1. The BE of Zn (2p) and O (1s) signals increase gradually with the Ag content for doped samples and more significantly deviates from that of stoichiometric ZnO values. This can be due to the changes in the charge-transfer efficiency between Zn^{2+} to O^{-2} ions, which is strongly affected by the structural defects leading to poorer charge transfer as also proposed by

others. Number of vacancies increase with the Ag addition. It is suggested that an increase in the number of oxygen vacancies with Ag addition. A thorough investigation of Ag (3d) signals in high-resolution spectra Figure 5.16 provide additional insights into the chemical nature of doping. The Ag ($3d_{5/2}$) and Ag ($3d_{3/2}$) peaks (~366 and ~372 eV) were observed for Ag/ZnO samples. The BE's for Ag (3d) signals are also summarized in Table 5.1. This can be attributed to the interaction between Ag and ZnO crystal. During the interaction, the free electrons on the level of the Ag could tunnel through the empty region within ZnO crystal. Therefore, the interaction between Ag and ZnO crystal results in the formation of a higher valance for Ag. The positional shift indicates the formation of an oxide layer on Ag particle surface. The splitting in the BE's of Ag ($3d_{5/2}$) and Ag ($3d_{3/2}$) signals shows that Ag were mainly in the metallic state (Ag^0).

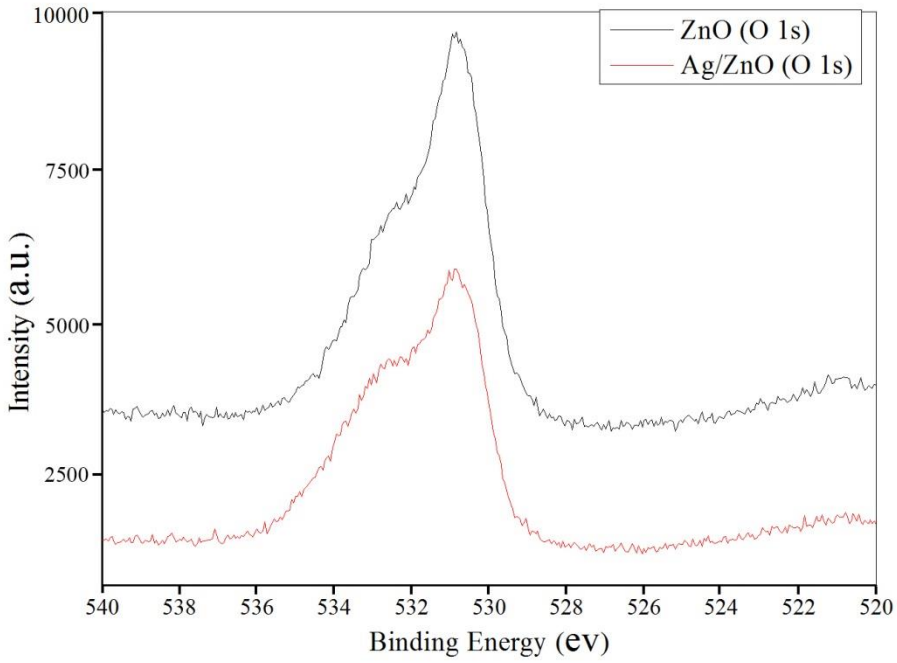

Figure 5.14. O (1s) XPS spectra of pure ZnO and Ag/ZnO nanoparticles

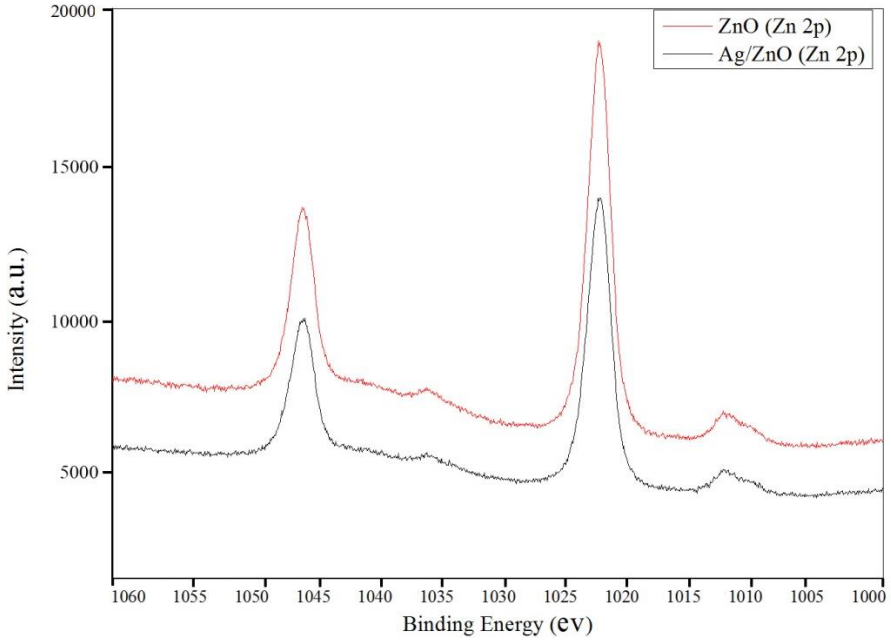

Figure 5.15. Zn (2p) XPS spectra of pure ZnO and Ag/ZnO nanoparticle

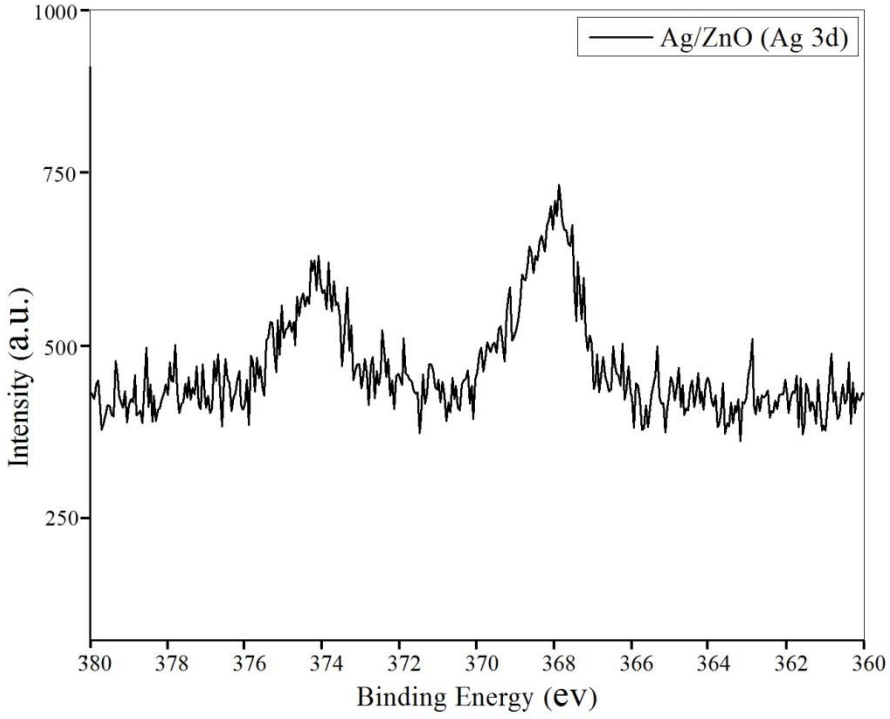

Figure 5.16. Ag (3d) XPS spectra of pure ZnO and Ag/ZnO nanoparticles

Table 5.2. Binding energy values (in eV) of Zn ($2p_{3/2}$), Zn ($2p_{1/2}$), O (1s) (lattice and chemisorbed oxygen), Ag ($3d_{5/2}$), and Ag ($3d_{3/2}$) for Ag/ZnO nanoparticles

Binding Energy (eV)						
	Zn ($2p_{3/2}$)	Zn ($2p_{1/2}$)	O (1s)*	O (1s)$^{\gamma}$	Ag ($3d_{5/2}$)	Ag ($3d_{3/2}$)
Ag/ZnO Particles	1021.59	1044.69	529.83	531.27	366.20	372.18
ZnO Particles	1021.41	1044.48	529.57	530.95	-	-

*lattice oxygen

$^{\gamma}$ chemisorbed oxygen

The corresponding binding energies for the Zn (2p), O (1s), and Ag (3d) signals, as determined from these high-resolution scans are summarized in Table 5.1.

5.4. Characterization of Unsaturated Polyester Resin (UPR)

5.4.1. Rheological Properties

As seen in Figure 5.17 polyester sample prepared with Ag, MgO, CaO particles did not show a shear thickening effect. The TiO_2 and ZnO prepared polyester sample showed an decrement in viscosity as increasing shear rate.

Flow behaviour can completely change with addition of filler or reinforced material to the composite (Hanemann 2006). The use of 5 wt% of the antibacterial agents cause decrement in viscosity but these variations are too small to cause any change in the stone.

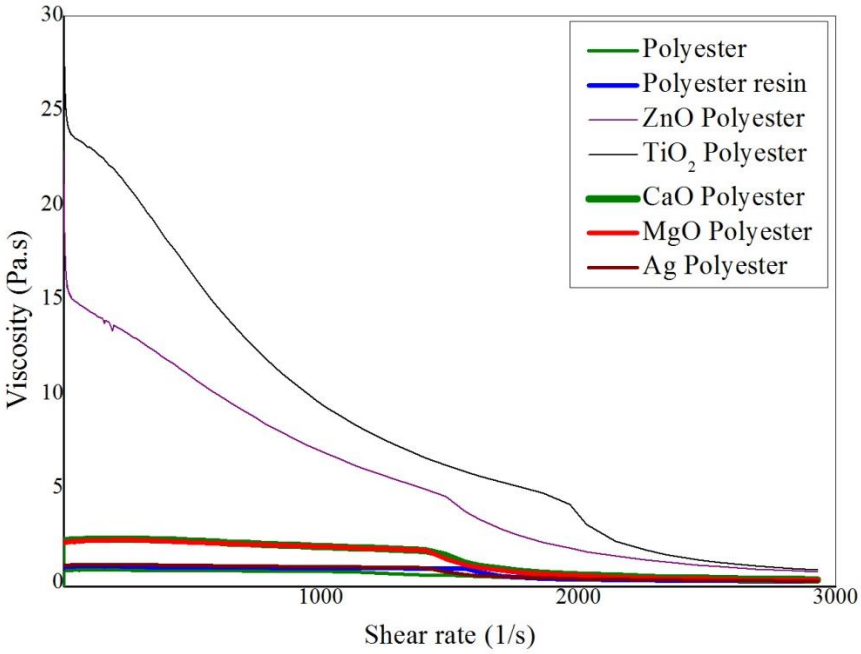

Figure 5.17 Rheology of polyester sample prepared with antibacterial agent

5.4.2. Scanning Electron Microscopy (SEM)

SEM images of polyester resin with silver, silver doped zincoxide, zincoxide, titanium dioxide, magnesiumoxide nanoparticles are shown in Figure 5.18, 5.19, 5.20, 5.21, 5.22 5.22, respectively.

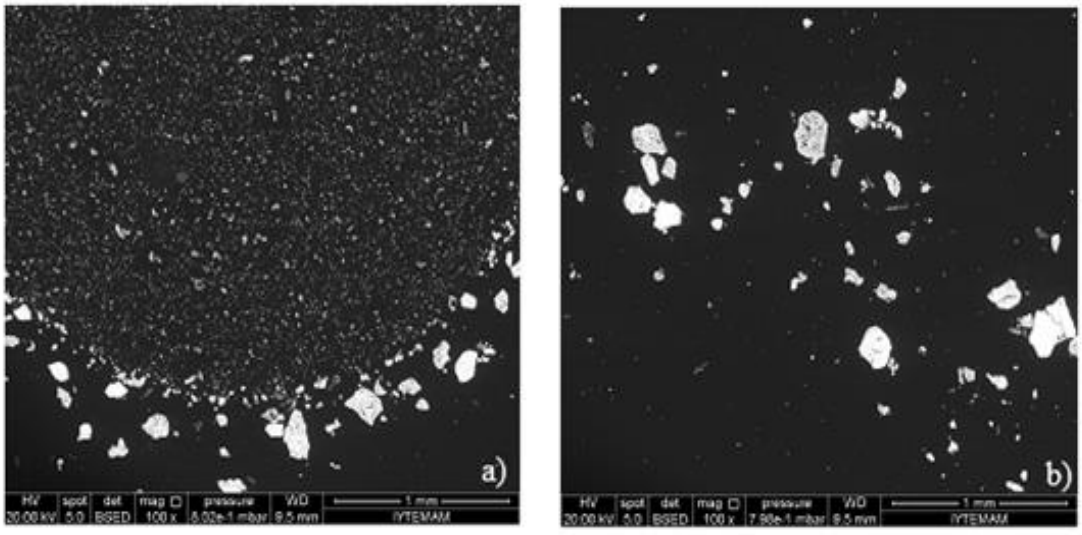

Figure 5.18. SEM images of Ag/Polyester resin a) 100 x, b**)** 100 x magnification

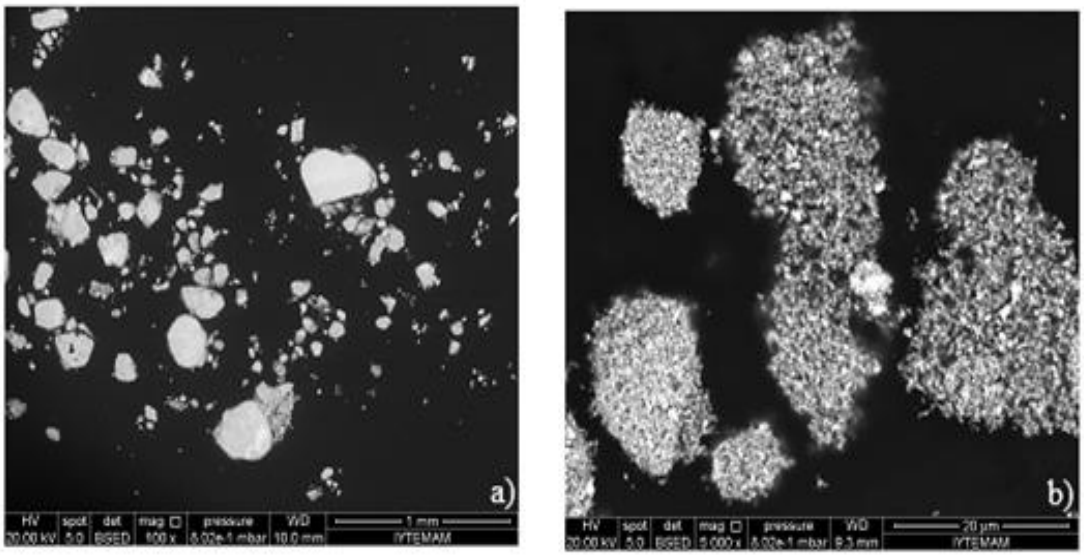

Figure 5.19. SEM images of Ag doped ZnO/Polyester resin a) 100 x, b) 5 000 x magnification

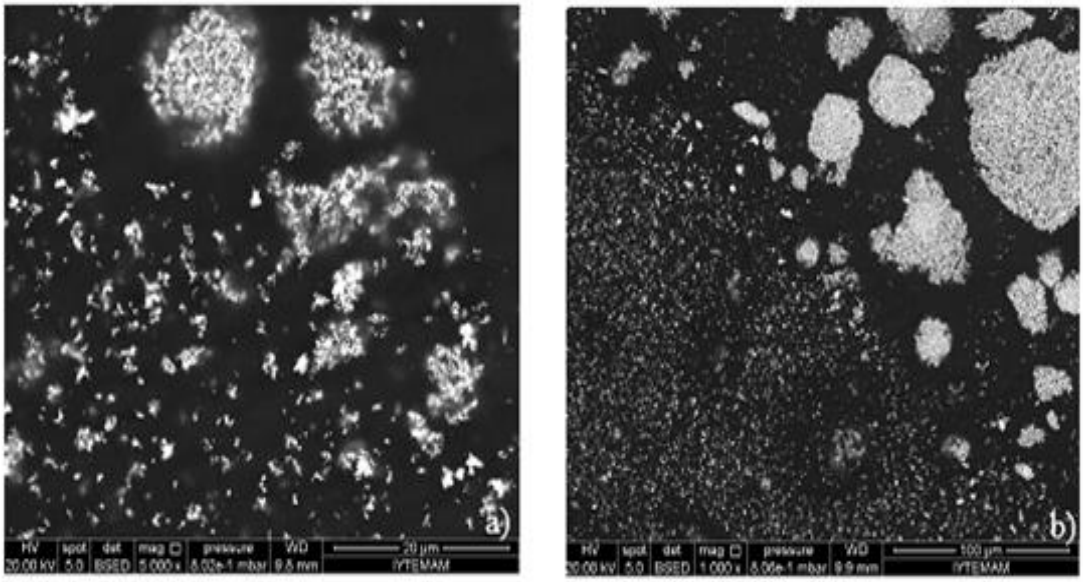

Figure 5.20. SEM images of ZnO/Polyester resin a) 5 000 x, b) 1 000 x magnification

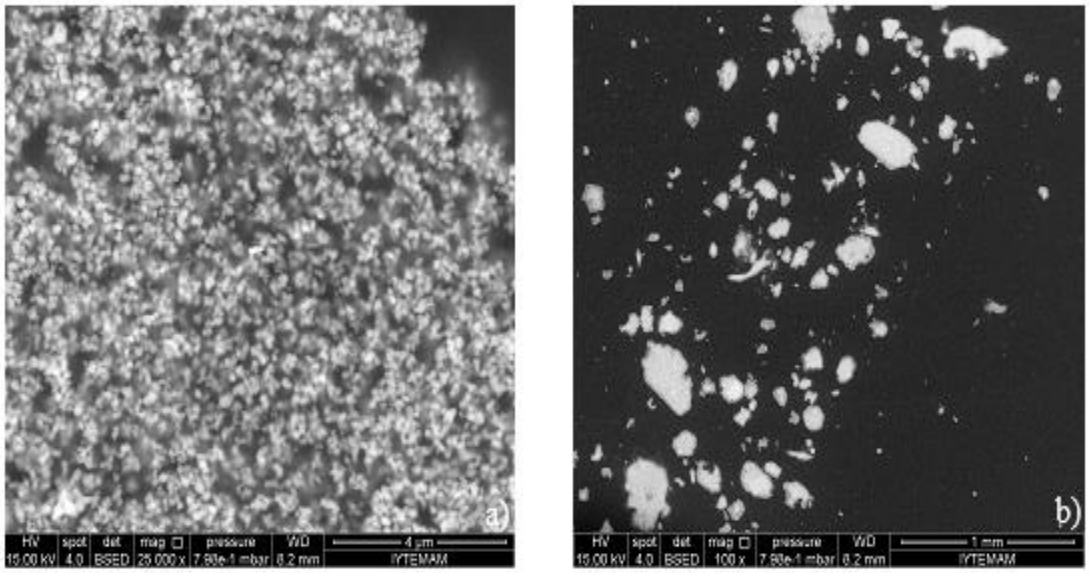

Figure 5.21. SEM images of Ti(IV)O2/Polyester resin a) 5 000 x, b) 1 000 x magnification

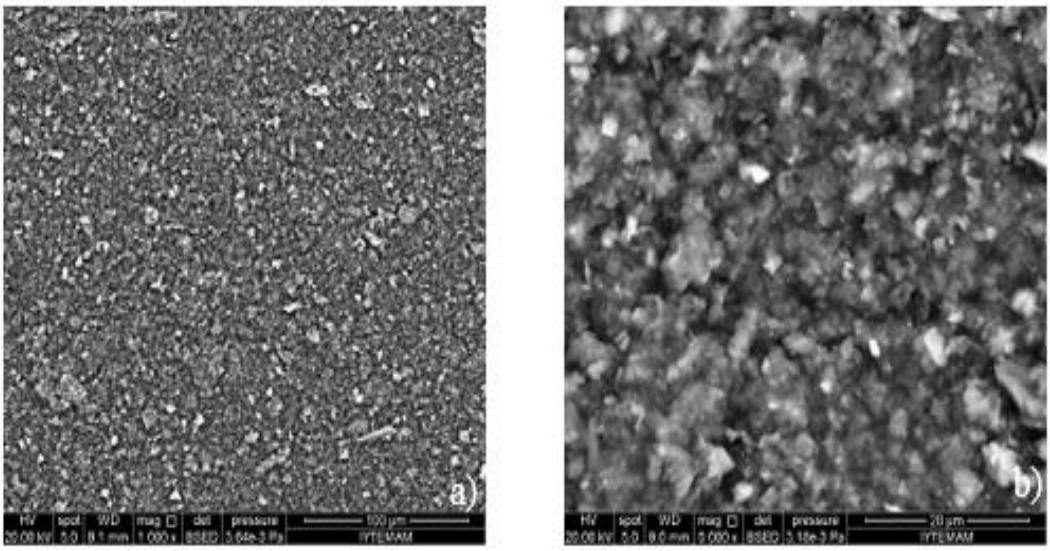

Figure 5.22. SEM images of MgO/Polyester resin a) 1 000 x, b) 5 000 x magnification

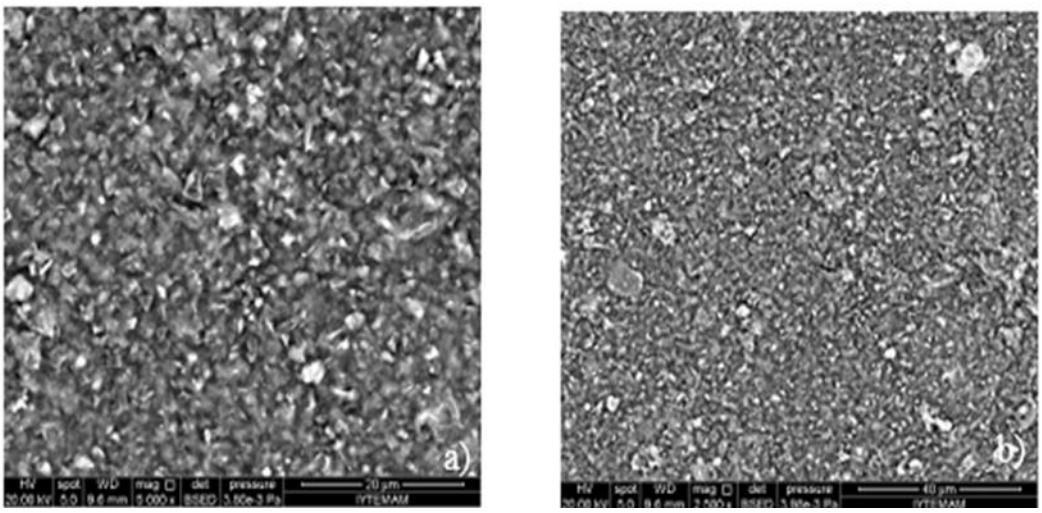

Figure 5.23. SEM images of CaO/Polyester resin a) 5 000 x, b**)** 2 500 x magnification

5.4.3. Fourier Transform Infrared Spectroscopy (FTIR)

As a mentioned before, unsaturated polyester which occurred because of copolymerization of styrene and polyester was provided from AKG Yalıtım ve İnşaat Malzemeleri San. ve Tic. A.Ş.

All the spectra were normalized to the unsaturated polyester absorption at 1730 cm^{-1} shown in Fig. 5.24. Styrene absorptions are indicated at 1495, 778 and 701 cm^{-1} (Pucić, 2003).

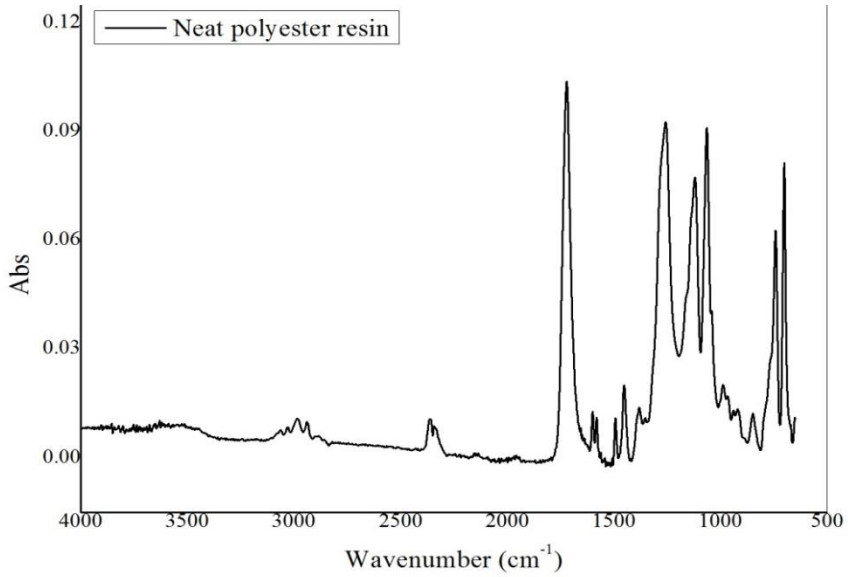

Figure 5.24. FTIR graph for unsaturated polyester

5.4.4. Thermal Properties

5.2.4.1. Thermogravimetric Analysis (TGA)

Thermal Gravimetric Analysis of (TGA) Ag Polyester, $Ti(IV)O_2$ polyester, ZnO polyester and Ag/ZnO polyester composites were made by Perkin Elmer Diamond TG/DTA Thermal Gravimetric Analyser. All composites were heated 30 ^oC to 640 ^oC by the rate of 10 ^oC/min. In order to provide effect of oxigen in the air for composites, nitrogen gas were used by the rate of 20 ml/min.

The weight loss started at around 230^oC, and the 99 % of the unsaturated polyester resin (UPR) was lost at around 390^oC. The mass loss occurs at two steps. The first and the sharp decrease in the mass occurred at between 230 and 390 ^oC. The second and the slow mass loss step was observed around 380 - 600 ^oC. TGA thermogram for Ag/Polyester, ZnO/Polyester, TiO_2/Polyester and Ag doped ZnO/Polyester are shown in Figure 5.25. TGA thermogram for MgO/Polyester and CaO/Polyester are shown in Figure 5.26.

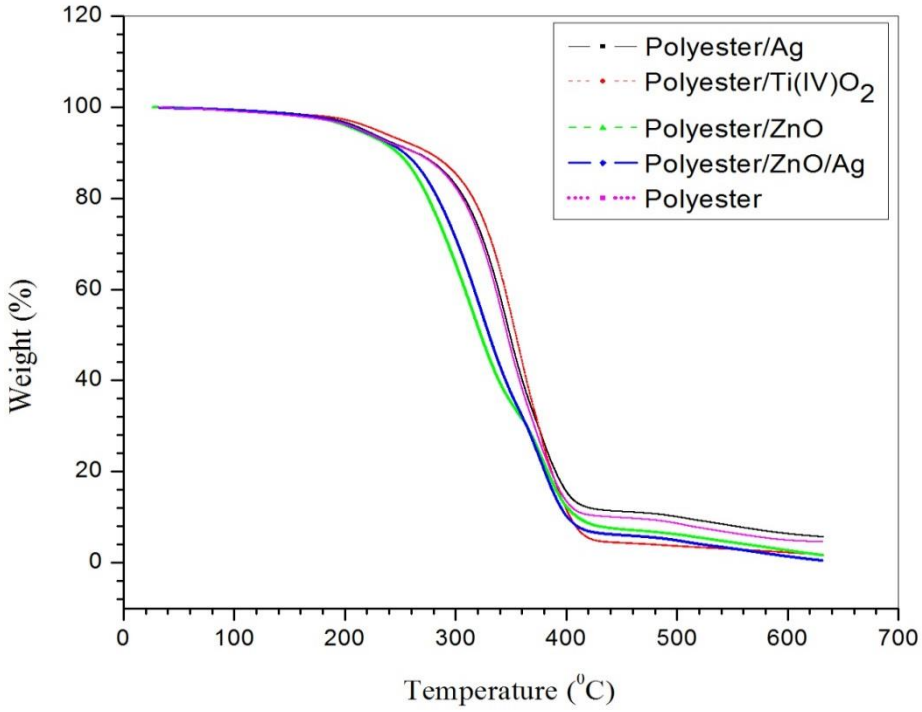

Figure 5.25. TGA thermogram for Ag/Polyester, ZnO/Polyester, TiO_2/Polyester and Ag doped ZnO/Polyester

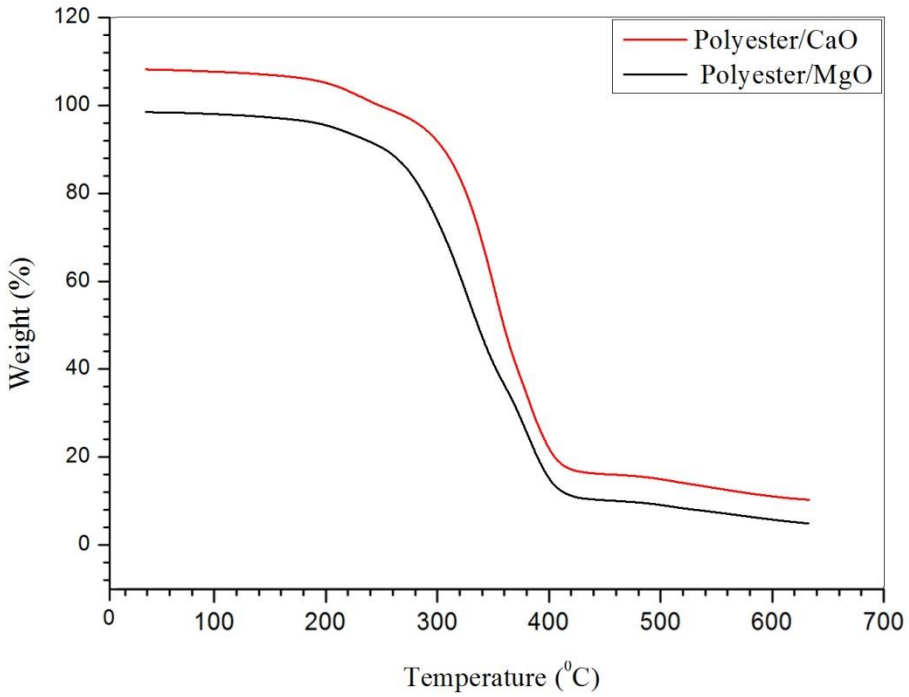

Figure 5.26. TGA thermogram for MgO/Polyester and CaO/Polyester

Table 5.3. Mass loss (%) of composite materials obtained according to TGA result

Materials	UPR Ag	UPR $Ti(IV)O_2$	UPR ZnO	UPR Ag/ZnO	UPR CaO	UPR MgO	UPR
Mass loss %	96.71	97.72	98.30	97.6	98.87	97.84	99.0

5.2.4.2. Differential Scanning Calorimeter (DSC)

Thermal behavior of polyester with different antibacterial particles was carried out by using differential scanning calorimeter (DSC). Glass Transition temperature is one of the most important of any polyester which is thermosetting materials chemically crosslink during the curing process.The final cured polyester materials does not melt when heated,but undergoes a slight softening (phase change) at elevated temperature. The ultimate T_g is determined by a number of factors: the chemical structure of polyester resin, the type of hardener and the degree of cure. Ag Ag/ZnO, ZnO, TiO_2, MgO, CaO polyester were heated 50.0 ^oC to 300.00 ^oC by the rate of 10 ^oC/min. For the polyester material, the reported T_g would be around 60-70^0C for all material with nanoparticles. T_g degree of polyester are not effected by antibacterial particles because

the amount of particle is too samall comparing to whole structure. Also, it was observed that decomposition peaks are shown after 350 ^{o}C. DSC thermograms for all antibacterial polyester are shown in Table 5.27.

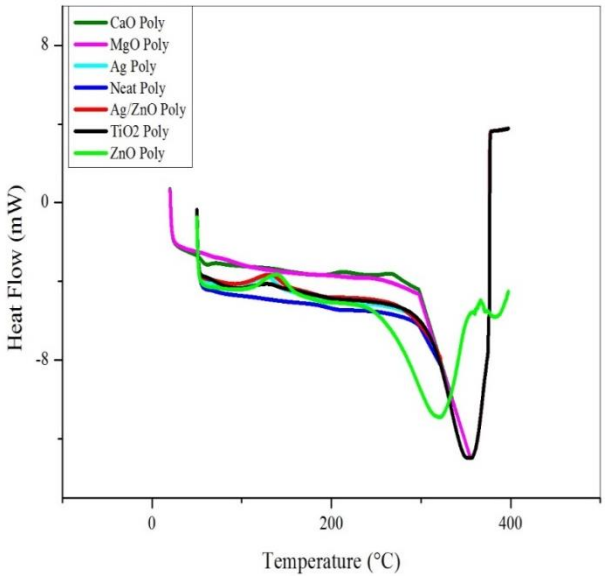

Figure 5.27. DSC thermograms for all antibacterial polyester

Table 5.4. Analysis of decomposition temparature and glass transition temparature (Tg) of Ag Polyester, Ti(IV)O_2 Polyester, ZnO Polyester, Ag/ZnO Polyester, neat Polyester resin

Materials	Tg (^{0}C)	Decomposotion Temperature (^{0}C)
ZnO Polyester	63.66	350.11
Ag Polyester	67.34	370.60
Ag/ZnO Polyester	69.56	371.68
TiO_2 Polyester	63.74	380.00
Mgo Polyester	67.98	381.90
CaO Polyester	66.98	380.58
Polyester	69.70	370.49

T_g values of all polyester with antibacterial particles are obtained at around 60-70^{0}C. Also, decomposotion temperatures of all polyesters with antibacterial particle are shown after 350 ^{o}C.

5.4. Characterization of Composite Stone

5.4.1. Microstructural Features

5.4.2. Scanning Electron Microscopy (SEM)

Figure 5.28. Image of a) scanning electron microscope (SEM) equipment b) polyester samples into the sem equipment

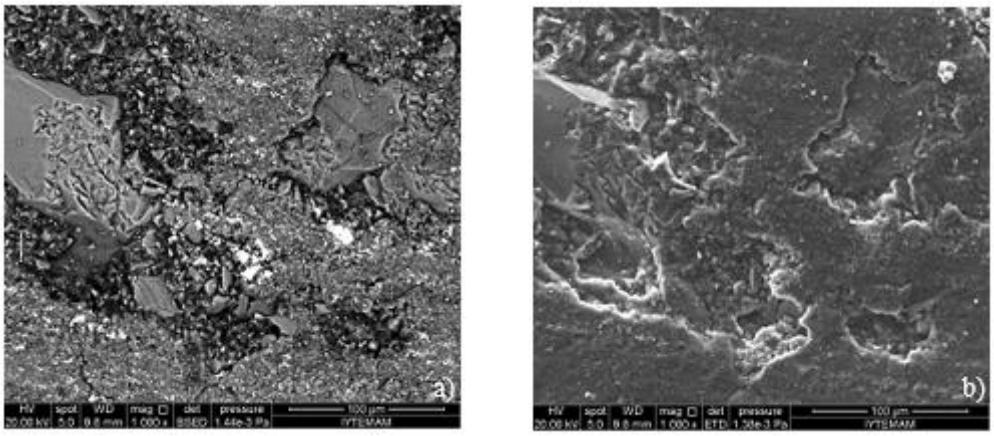

Figure 5.29. a) BSED images of Ag/UPR-quartz NCs stone (1 000 x), b) ETD images of Ag/UPR-quartz NCs stone (1 000 x)

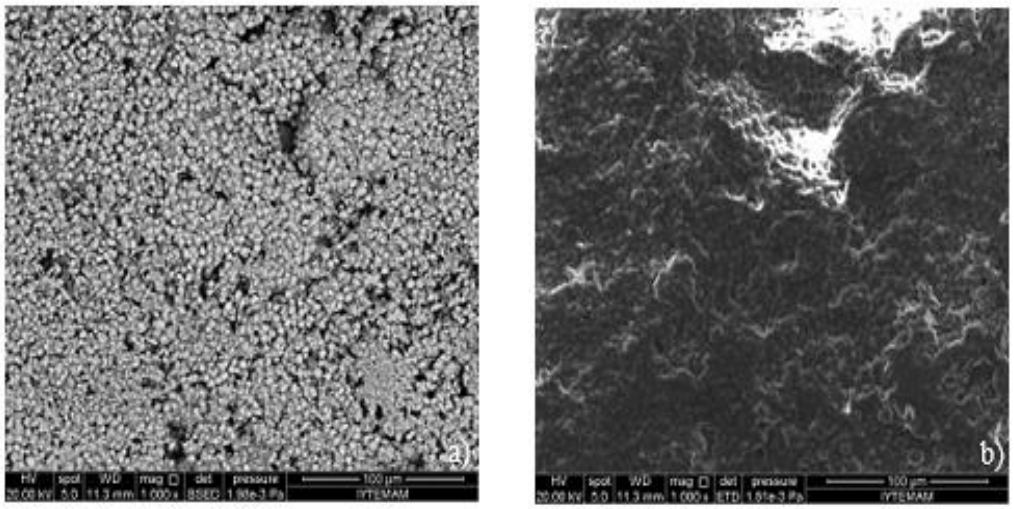

Figure 5.30. a) BSED images of CaO/UPR-quartz NCs stone (1 000 x), b) ETD images of CaO/UPR-quartz NCs stone (1 000 x)

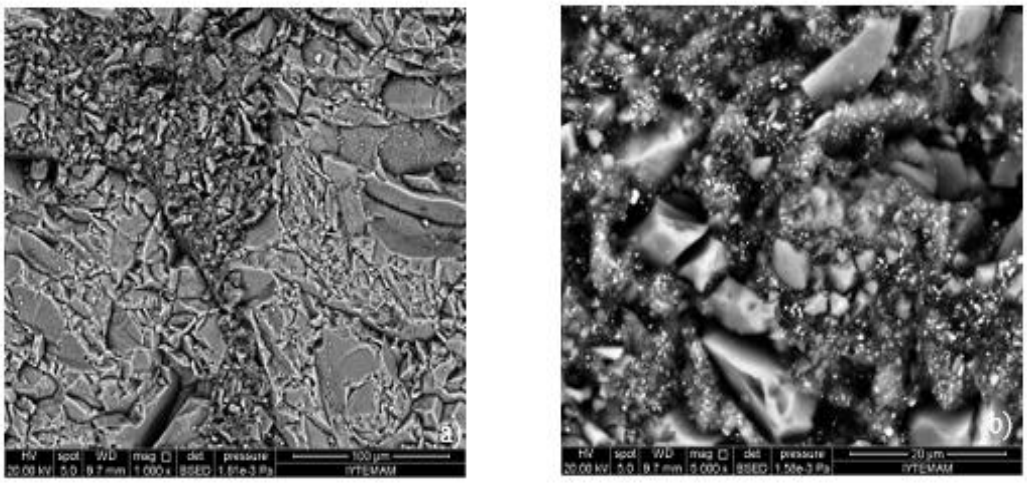

Figure 5.31. BSED images of a) MgO/UPR-quartz NCs stone (1 000 x), MgO/UPR-quartz NCs stone (5 000 x)

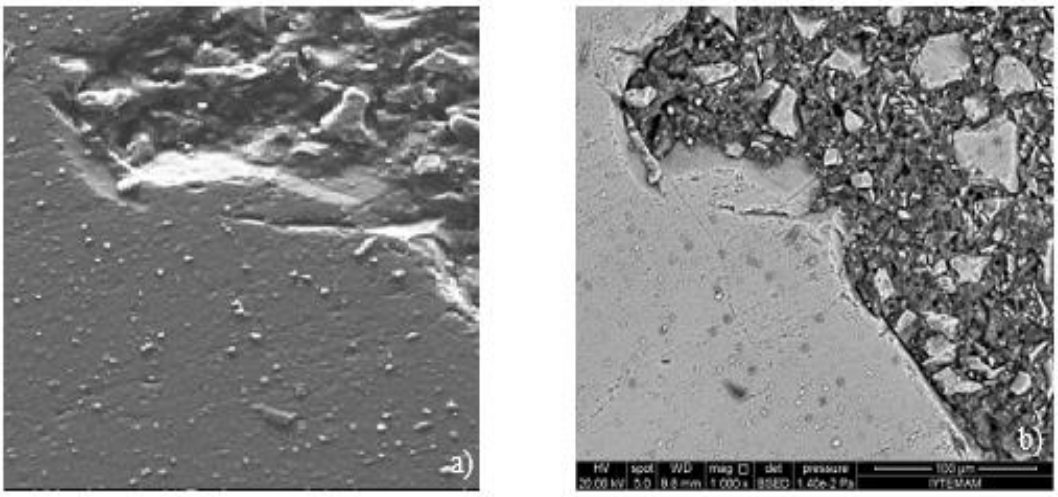

Figure 5.32. ETD images of TiO_2/UPR-quartz NCs stone (1 000 x), b) BSED images of TiO_2/UPR-quartz NCs stone (1 000 x)

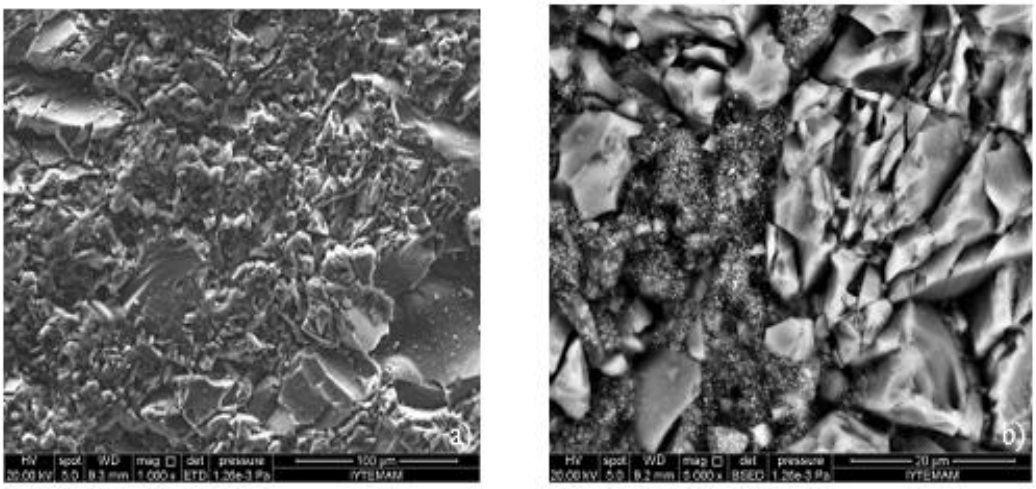

Figure 5.33. BSED images of a) ZnO/UPR-quartz NCs stone (1 000 x), ZnO/UPR-quartz NCs stone (5 000 x)

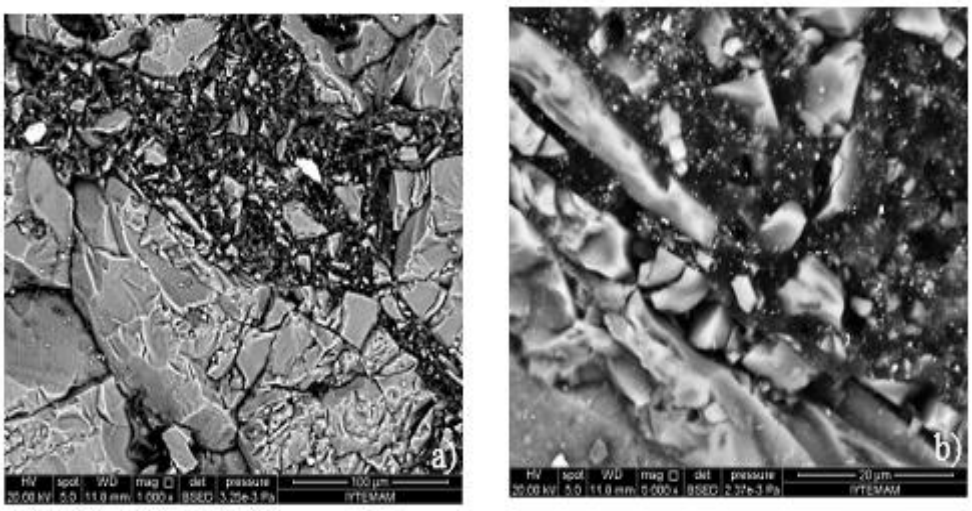

Figure 5.34. BSED images of a) Ag doped ZnO/UPR-quartz NCs stone (1 000 x), Ag doped ZnO/UPR-quartz NCs stone (5 000 x)

5.4.3. Mechanical Property Characterization

5.3.3.1. Flexure Testing

Table 5.4.Flexural properties of neat stone

Sample ID	Maximum flexure load (N)	Flexure stress at maximum flexure load (MPa)	Thickness (nm)	Energy at break (J)	Rate (MPa/s)	Support span (mm)
1	1139	52.4	10.76	0.618	0.250	180.00
2	1063	53.3	10.26	0.494	0.250	180.00

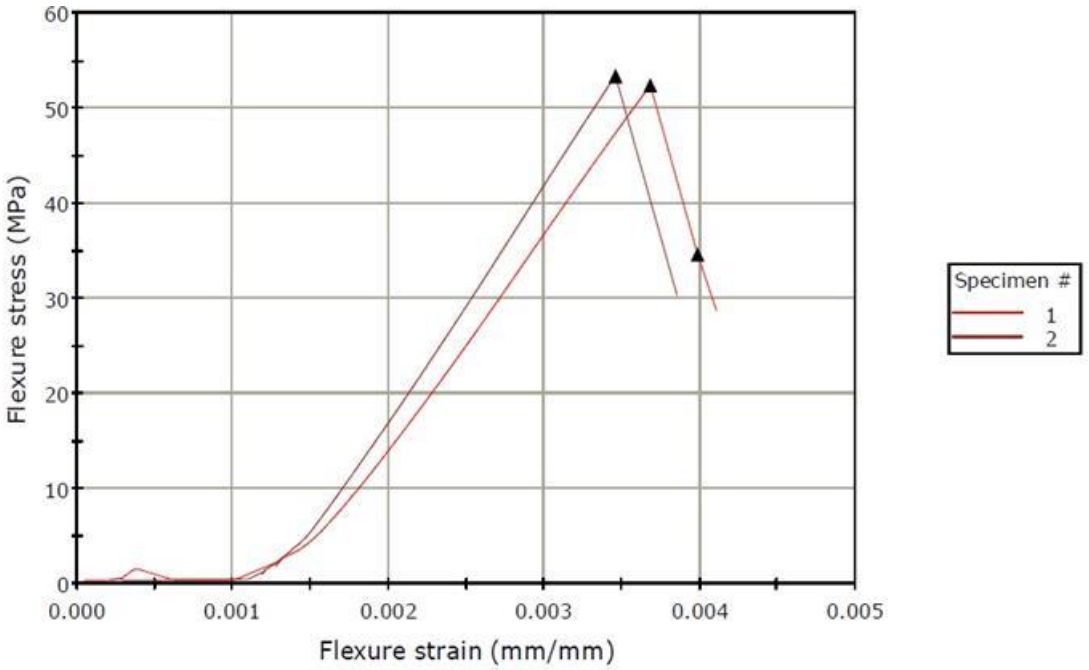

Figure 5.35. Flexure stress vs. strain graphs of neat composite stone

Table 5.5. Flexural properties of Ag/ZnO stone

Sample ID	Maximum flexure load (N)	Flexure stress at maximum flexure load (MPa)	Thickness (nm)	Energy at break (J)	Rate (MPa/s)	Support span (mm)
1	1069	52.5	10.37	0.618	0.250	180.00
2	999	44.5	10.88	0.494	0.250	180.00

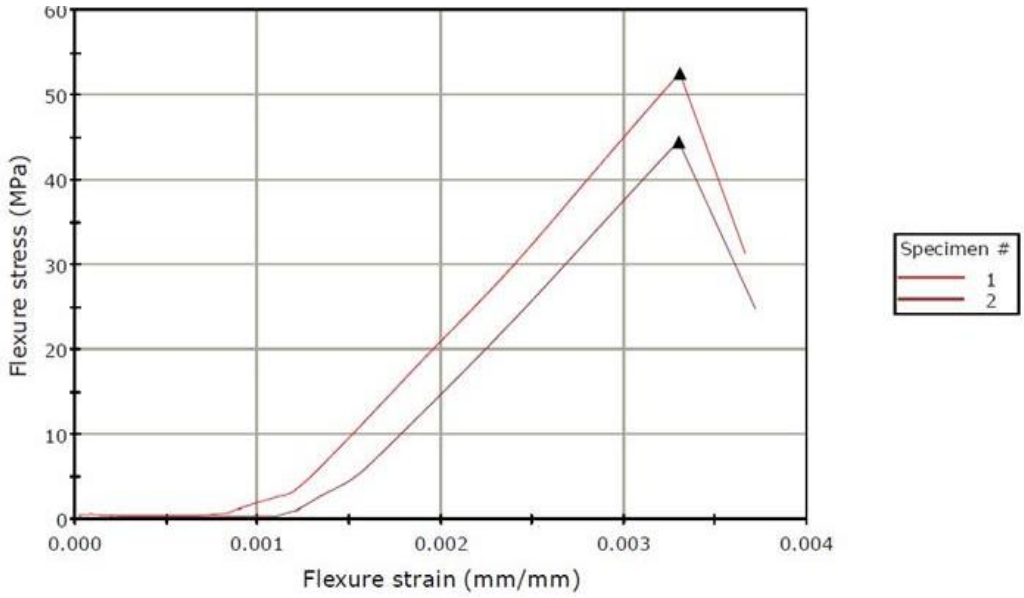

Figure 5.36. Flexure stress vs. strain graphs of Ag/ZnO added composite stone

Table 5.6. Flexural properties of ZnO stone

Sample ID	Maximum flexure load (N)	Flexure stress at maximum flexure load (MPa)	Thickness (nm)	Energy at break (J)	Rate (MPa/s)	Support span (mm)
1	989	47.9	10.45	0.489	0.250	180.00
2	1003	45.6	10.80	0.488	0.250	180.00

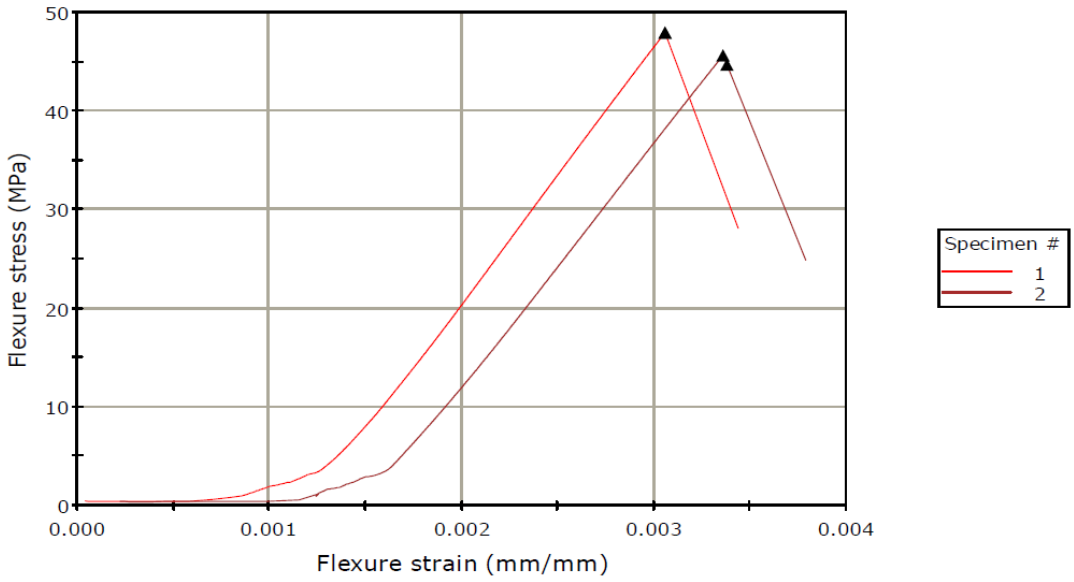

Figure 5.37. Flexure stress vs. strain graphs of ZnO added composite stone

Table 5.7. Flexural properties of Ag stone

Sample ID	Maximum flexure load (N)	Flexure stress at maximum flexure load (MPa)	Thickness (nm)	Energy at break (J)	Rate (MPa/s)	Support span (mm)
1	1359	46.4	12.57	1.892	0.250	180.00
2	1690	61.7	12.15	1.287	0.250	180.00

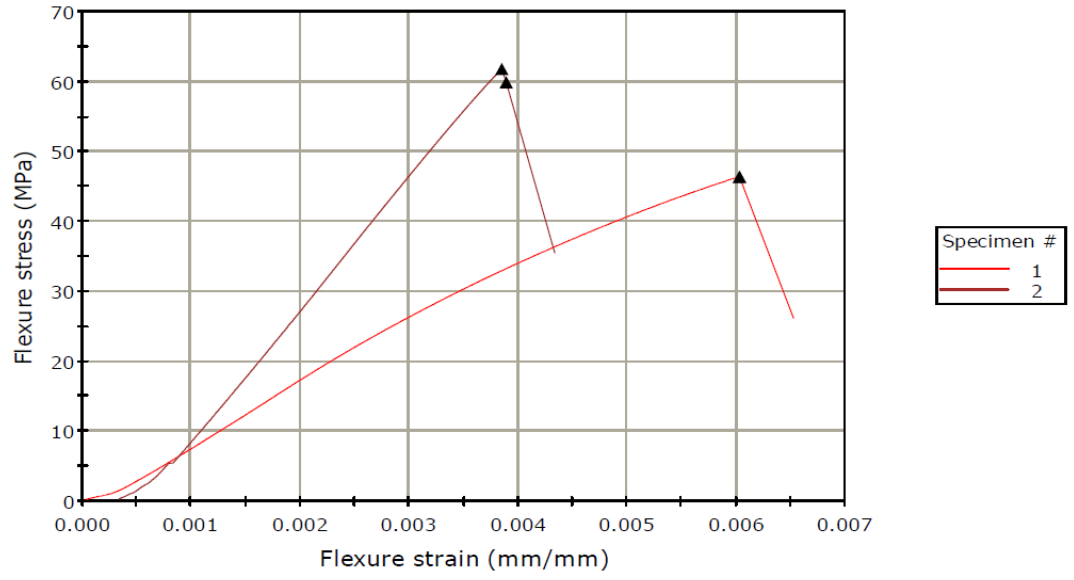

Figure 5.38. Flexure stress vs. strain graphs of Ag added composite stone

Table 5.8. Flexural properties of TiO2 stone

Sample ID	Maximum flexure load (N)	Flexure stress at maximum flexure load (MPa)	Thickness (nm)	Energy at break (J)	Rate (MPa/s)	Support span (mm)
1	1145	53.2	10.69	0.659	0.250	180.00
2	1097	53.4	10.43	0.635	0.250	180.00

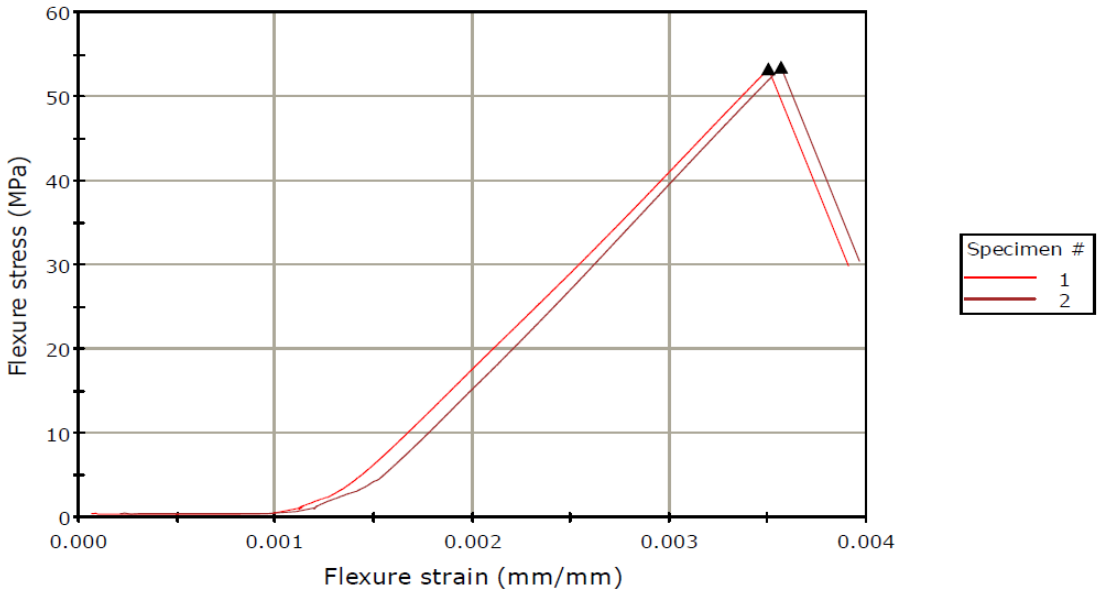

Figure 5.39. Flexure stress vs. strain graphs of TiO_2 added composite stone

Table 5.9. Flexural properties of MgO stone

Sample ID	Maximum flexure load (N)	Flexure stress at maximum flexure load (MPa)	Thickness (nm)	Energy at break (J)	Rate (MPa/s)	Support span (mm)
1	711	33.0	10.76	0.229	0.250	180.00
2	211	8.5	11.53	0.563	0.250	180.00

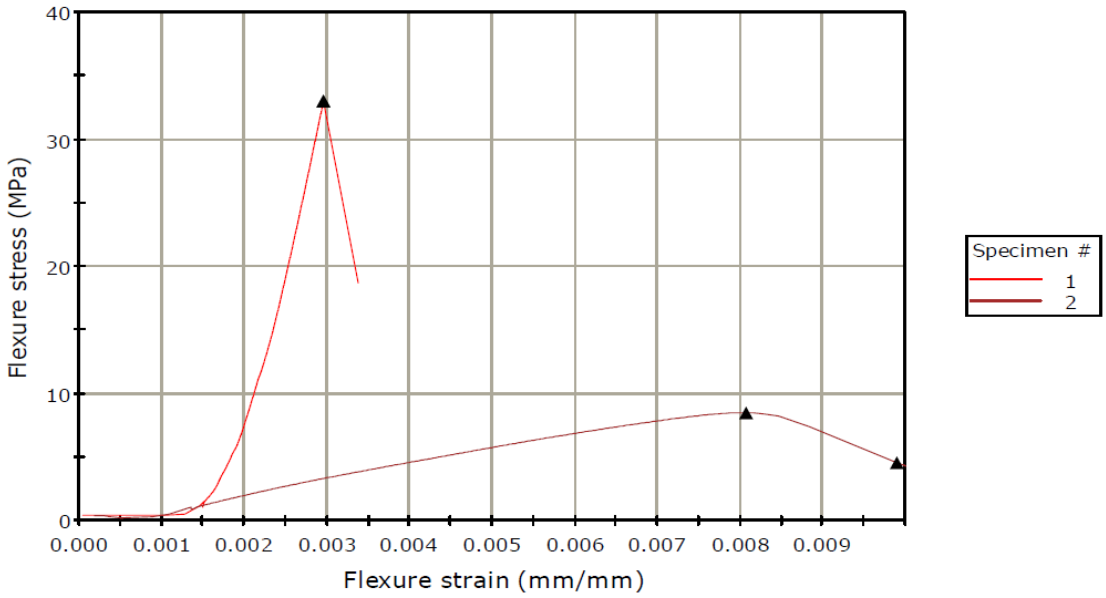

Figure 5.40. Flexure stress vs. strain graphs of MgO added composite stone

Table 5.10. Flexural properties of CaO stone

Sample ID	Maximum flexure load (N)	Flexure stress at maximum flexure load (MPa)	Thickness (nm)	Energy at break (J)	Rate (MPa/s)	Support span (mm)
1	1208	42.4	12.35	0.470	0.250	180.00
2	1310	46.7	12.31	0.520	0.250	180.00

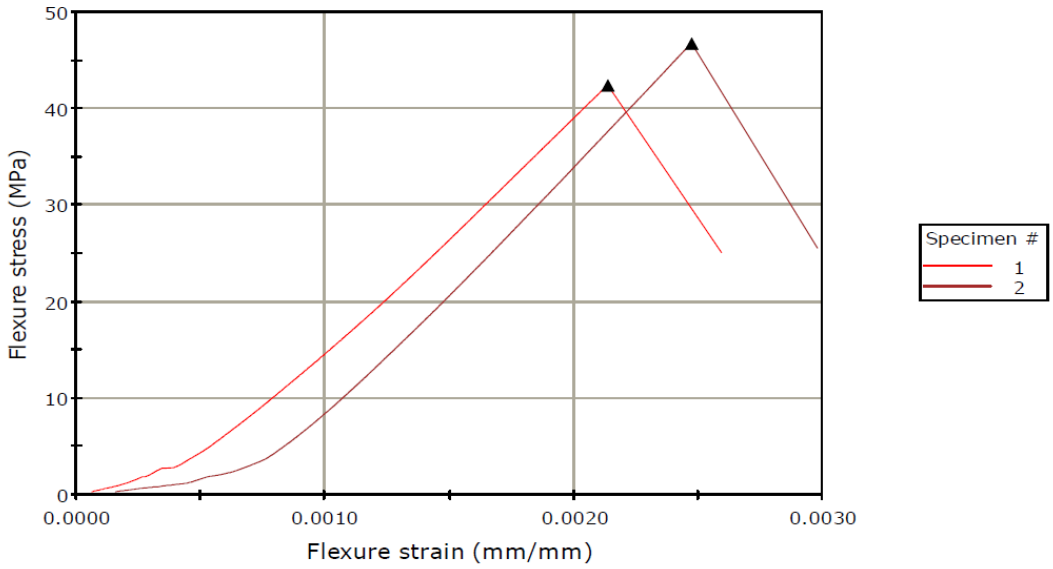

Figure 5.41. Flexure stress vs. strain graphs of CaO added composite stone

5.3.3.2. Impact Resistance

In order to find the impact resistance, impact test using steel ball is performed. The steel balls were dropped at the height of 10-60 cm with the range of 5 cm. Neat, Ag loaded, ZnO loaded, Ag/ZnO loaded, Ti(IV)O_2 loaded, Ti(IV)O_2 loaded and CaO loaded composites are failed at 2.94 joule but MgO loaded composites are failed 5.88 joule. It is said that MgO stone more durable than the other but this powder changes the standart stone structure so it is not useful fort this study.

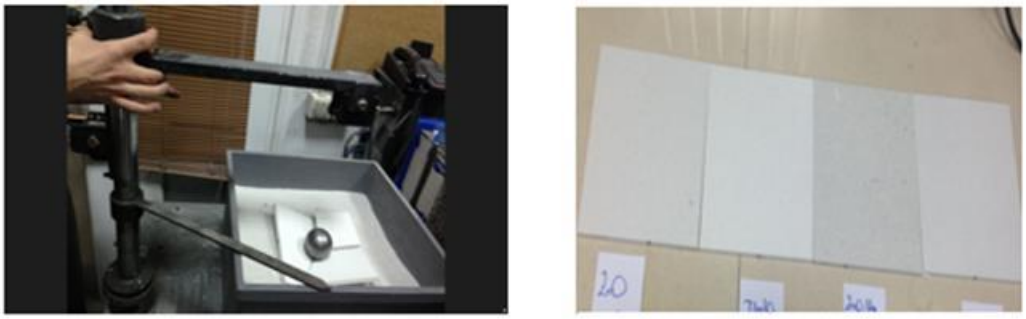

Figure 5.42. Images of composites b) before and a) after impact test

Table 5.11. Impact resistance test results for the composites

Energy value corresponding to height of released ball / Test Specimen	30 cm versus 2.94 Joule	60 cm versus 5.88 Joule
Neat composites	failed	not failed
Ag loaded composites	failed	not failed
ZnO loaded composites	failed	not failed
Ag/ZnO loaded composites	failed	not failed
Ti(IV)O_2 loaded composites	failed	not failed
MgO loaded composites	not failed	failed
CaO loaded composites	failed	not failed

5.4. Antibacterial Activity Tests

Antibacterial activities of polyesters, and polyester-quartz composites containing Ag, ZnO, Ag/ZnO, Ti(IV)O_2, MgO, and CaO were tested against *E.coli* and *B. subtilis*. Polyester materials containing 5% of each Ag, CaO, Ag/ZnO, ZnO, MgO and TiO_2 presented antibacterial activity against *E.coli* corresponding to 80%, 76%, 64%, 54%, 47% and 29%, respectively (Table5.12) Antibacterial activity against *B.subtilis* exhibited by the same materials was 78%, 71%, 57%, 50%, 43% and 23%, respectively (Table5.13). For the antibacterial nanocomposite stones, the highest antibacterial activity was observed for 5% polyester Ag and CaO composite stones which showed over 87% and 86 % reduction in *E. Coli* bacterial numbers, respectively (Table5.14). Antibacterial activity of 5%Ag and 5% CaO composite stones was observed over 78 and 73% reduction in *B.subtilis* bacterial numbers, respectively (Table5.15). Antibacterial activitiy of 5% silver doped zincoxide composite stones was almost the same compared with 5 % zincoxide composite stones, against both *E.coli* (Table 5.14), *B.subtilis* (Table 5.15). Nanocomposite stones containing either MgO or TiO_2, had antibacterial activities less than 50% against both *E.coli* and *B.subtilis* (Table 5.14, Table 5.15).

Table 5.12. Antibacterial test result of polyester and antibacterial agent added polyester materials against *E.coli*

Test Specimen	**Bacterial amount (cfu / ml)** **Contact time " 24 saat "**	**%**
1. Polyester	13,06 x 10^5	9,56
2. Polyester	13,13 x 10^5	9,07
3. 1% Ag Polyester	11,00 x 10^5	23,82
4. 3% Ag Polyester	3,79 x 10^5	**73,75**
5. 5% Ag Polyester	2,87 x 10^5	**80,12**
6. 1% ZnO Polyester	12,57 x 10^5	12,95
7. 3% ZnO Polyester	9,24 x 10^5	36,01
8. 5% ZnO Polyester	6,62 x 10^5	54,15
9. 1% TiO_2 Polyester	13,00 x 10^5	9,97
10. 3% TiO_2 Polyester	12,60 x 10^5	12,74
11. 5% TiO_2 Polyester	10,20 x 10^5	29,36
12. 1% Ag/ZnO Polyester	11,90 x 10^5	17,59
13. 3% Ag/ZnO Polyester	10,11 x 10^5	48,75
14. 5% Ag/ZnO Polyester	5,10 x 10^5	**64,68**
15. 1% CaO Polyester	11,10 x 10^5	23,13
16. 3% CaO Polyester	7,19 x 10^5	**50,20**
17. 5% CaO Polyester	3,40 x 10^5	**76,45**
18. 1% MgO Polyester	12,8 x 10^5	11,35
19. 3% MgO Polyester	10,5 x 10^5	27,28
20. 5% MgO Polyester	7,65 x 10^5	47,02
21. Control	14,44 x 10^5	–

Table 5.13. Antibacterial test result of polyester and antibacterial agent added polyester materials against *B.subtilis*

Test Specimen	**Bacterial amount (cfu / ml) Contact time " 24 saat "**	**%**
1. Polyester	12,60 x 10^5	10,00
2. Polyester	12,52 x 10^5	10,57
3. 1% Ag Polyester	11,10 x 10^5	20,71
4. 3% Ag Polyester	3,95 x 10^5	**71,78**
5. 5% Ag Polyester	3,02 x 10^5	**78,42**
6. 1% ZnO Polyester	13,00 x 10^5	7,14
7. 3% ZnO Polyester	10,05 x 10^5	28,20
8. 5% ZnO Polyester	7,00 x 10^5	**50,00**
9. 1% TiO_2 Polyester	13,15 x 10^5	6,07
10. 3% TiO_2 Polyester	12,95 x 10^5	7,50
11. 5% TiO_2 Polyester	10,65 x 10^5	23,90
12. 1% Ag/ZnO Polyester	12,20 x 10^5	12,80
13. 3% Ag/ZnO Polyester	9,80 x 10^5	30,00
14. 5% Ag/ZnO Polyester	6,00 x 10^5	**57,14**
15. 1% CaO Polyester	11,50 x 10^5	17,85
16. 3% CaO Polyester	7,86 x 10^5	**43,08**
17. 5% CaO Polyester	4,00 x 10^5	**71,40**
18. 1% MgO Polyester	13,0 x 10^5	7,14
19. 3% MgO Polyester	10,80 x 10^5	22,80
20. 5% MgO Polyester	7,85 x 10^5	43,90
21. Control	14,00 x 10^5	–

Table 5.14. Antibacterial test result of composite stone and antibacterial composite stone against *E.coli*

Test Specimen	**Bacterial amount (cfu / ml)** **Contact time " 24 saat "**	**%**
1. Stone	12,46 x 10^5	10,35
2. Stone	12,40 x 10^5	10,79
3. 1% Ag Stone	8,85 x 10^5	36,33
4. 3% Ag Stone	2,95 x 10^5	**78,77**
5. 5% Ag Stone	1,80 x 10^5	**87,00**
6. 1% ZnO Stone	10,54 x 10^5	24,14
7. 3% ZnO Stone	6,20 x 10^5	**55,39**
8. 5% ZnO Stone	2,67 x 10^5	**80,79**
9. 1% TiO_2 Stone	11,68x 10^5	15,97
10. 3% TiO_2 Stone	10,74 x 10^5	22,73
11. 5% TiO_2 Stone	7,60 x 10^5	45,30
12. 1% Ag/ZnO Stone	9,70 x 10^5	30,21
13. 3% Ag/ZnO Stone	6,06 x 10^5	**56,40**
14. 5% Ag/ZnO Stone	2,54 x 10^5	**81,72**
15. 1% CaO Stone	10,32 x 10^5	25,75
16. 3% CaO Stone	4,70 x 10^5	**66,18**
17. 5% CaO Stone	1,90 x 10^5	**86,30**
18. 1% MgO Stone	11,80 x 10^5	15,10
19. 3% MgO Stone	9,80 x 10^5	29,49
20. 5% MgO Stone	6,85 x 10^5	50,71
21. Control	13,90 x 10^5	–

Table 5.15. Antibacterial test result of composite stone and antibacterial composite stone against *B. Subtilis*

Test Specimen	**Bacterial amount (cfu / ml) Contact time " 24 saat "**	**%**
1. Stone	13,00 x 10^5	9,34
2. Stone	13,03 x 10^5	9,13
3. 1% Ag Stone	10,48 x 10^5	26,91
4. 3% Ag Stone	4,64x 10^5	**67,64**
5. 5% Ag Stone	3,12 x 10^5	**78,20**
6. 1% ZnO Stone	12,58 x 10^5	12,27
7. 3% ZnO Stone	8,37 x 10^5	41,63
8. 5% ZnO Stone	3,87 x 10^5	**73,01**
9. 1% TiO_2 Stone	12,67 x 10^5	11,64
10. 3% TiO_2 Stone	11,64 x 10^5	18,82
11. 5% TiO_2 Stone	10,83 x 10^5	24,47
12. 1% Ag/ZnO Stone	12,12 x 10^5	15,48
13. 3% Ag/ZnO Stone	8,14 x 10^5	43,23
14. 5% Ag/ZnO Stone	4,05 x 10^5	**71,75**
15. 1% CaO Stone	12,00 x 10^5	16,31
16. 3% CaO Stone	5,74 x 10^5	**59,97**
17. 5% CaO Stone	3,86 x 10^5	**73,08**
18. 1% MgO Stone	12,98 x 10^5	9,48
19. 3% MgO Stone	10,73 x 10^5	25,17
20. 5% MgO Stone	7,93 x 10^5	44,70
21. Control	14,34 x 10^5	–

5.4.1. Inductively Coupled Plasma Spectrometer (ICP)

ICP AES spectroscopy was used to determine the extent of Ag, ZnO, Ag/ZnO, MgO, CaO and TiO_2 particles dissolved in buffer solution from antibacterial polyester based nanocomposite stone by analyzing the liquid phase. (Table 5.16).

Table 5.16. Antibacterial particles dissolved in buffer solution from antibacterial polyester based nanocomposite stone.

Element name	Amount of elemet (μg/L)
Mg	95.6
Ca	971
Ti	12.4
Zn	24.7
Ag	4.84

CHAPTER 6

CONCLUSIONS

Characterization of nanoparticles includes microstructural features, X-Ray Diffraction (XRD), Scanning Electron Microscopy (SEM), Dynamic Light Scattering (DLS) and X-ray Photoelectron Spectroscopy (XPS) Techniques. The X-ray diffraction of the Ag nanoparticles suggested that silver existed purely in the face-centered cubic (fcc) structure, however the crystal structure of ZnO particles were polycrystalline wurtzite structure. Ag/ZnO particles which were produced by mixing of Ag and ZnO particles showed different crystalline structure. The morphologic behaviour of nanoparticles were investigated by SEM analysis. Dynamic Light Scattering (DLS) showed the average particle size of nanoparticles. Particle sizes of powders were found to be between 110-340 nm. X-ray Photoelectron Spectroscopy (XPS) Technique was used to analyse the oxidation state of Ag on the ZnO surface. In order to manufacture a large stone, thermal and morphological behaviours of polyester- which is the matrix for stone- were investigated. The distribition of nanoparticles on polyester surface were shown by SEM analysis. There were some aggregates observed. To overcome this, effective mixing was achieved during stone production. Thermal behavior of polymer composites was analysed by differential scanning calorimeter (DSC). For the polyester material, the reported Tg would be 80^0C for all nanoparticles. Decomposition peaks were seen after 350 ^{o}C. The weight percentage of powder in polyester samples were measured by thermogravimetric analysis (TGA) method. TGA was also used for determination onset of degradation temperature, termination of degradation temperature and weight loss (%). Onset of degradation temperature, termination of degradation temperature of ZnO and Ag/ZnO polyesters was earlier than the other powders.

Mechanical property was characterized by flexure and impact testing. In order to determine the effect of powder addition to the flexibility of composites, flexibility test was performed. The results showed that, samples containing antibacterial agent, did not cause a significant reduction of flexure strength compared to the standart sample. Impact testing was performed to understand the characteristic of resistance to fracture

under sudden application of an exerted force. It was observed that, MgO stone was more resistant than the other antibacterial agents. However MgO powder deformed the standart stone structure, rendering it useless for this study.

Our results confirmed that, the antibacterial performances of both the stones, and the polyester based composites were enhanced significantly by the incorporation of Ag, ZnO, Ag doped ZnO and CaO nanoparticles aginst both *E. coli* and *B. Subtilis* with similar efficiencies. Overall there was around 2% lower antibacterial activity against *B. subtilis* which is Gram-positive compared with Gram-negative *E. coli* cells. This could be due to the differences between the cell walls of Gram-positive and Gram-negative bacteria. The peptidoglycan in the cell walls of Gram-positive bacteria is much thicker than in the Gram-negative bacteria (Feng, Wu et al. 2000). It is possible that, antibacterial agents penetrate the thicker cell less efficiently leading to a slightly decreased anti-bacterial effect on B. subtilis. However, the difference was minute. Our results also confirmed that, quartz which was used to prepare stones, contributed to the observed higher antibacterial activity of the stones compared to the polyester based nanocomposites which do not contain any quartz (Tables 5.12, 5.13, 5.14 and 5.15).

ICP AES spectroscopy was used to determine the extent of Ag, ZnO, Ag/ZnO, MgO, CaO and TiO_2 particles from the antibacterial polyester based nanocomposite stone dissolved in the buffer solution during the antibacterial test procedure. Analysis indicated that, small amounts of antibacterial particles were dissolved in the buffer suggesting the effect of the dissolved antibacterial powders on the antibacterial activity was minimal. Hence, the observed anti-bacterials were due to the presence of anti-bacterials agents incorporated into composite materials.

As a conclusion, The particle sizes were observed to be around 115, 296, 300, 190, 200, 210 nm for Ag, Ag/ZnO, ZnO, MgO, CaO, TiO_2 NPs, respectively. We used these nanomaterials to evaluate their antibacterial activity against both Gram-negative (*Escherichia coli*) and Gram-positive (*Bacillus subtilis*) bacteria. Among the metal oxide nanomaterials, Ag showed greatest antimicrobial activity against both Gram-positive and Gram-negative bacteria used in this study. It was observed that Ag nanoparticles had excellent bactericidal potential, while TiO_2 nanoparticles exhibited the least bactericidal activity. The order of antibacterial activity was demonstrated to be the following: Ag CaO Ag/ZnO, ZnO, MgO and TiO_2. Although Ag added stone had also good properties, its colour was darkened considerably causing it to be less desirable

compared to CaO containig stones. CaO stone showed the most desired total effect in terms of abrassive, impact, thermal and colour behaviour of the system.

REFERENCES

Amin, Shahab Ansari, Mohammad Pazouki, and Azarmidokht Hosseinnia. 2009. "Synthesis of TiO_2–Ag nanocomposite with sol–gel method and investigation of its antibacterial activity against *E. coli*." *Powder Technology* 196 (3):241-245.

Avila, Antonio F, Paulo Rodrigues, Dagoberto B Santos, and Ana CA Faria. 2003. "A dual analysis for recycled particulate composites: linking micro-and macro-mechanics." *Materials characterization* 50 (4):281-291.

Ba-Abbad, Muneer M, Abdul Amir H Kadhum, Abu Bakar Mohamad, Mohd S Takriff, and Kamaruzzaman Sopian. 2012. "Synthesis and Catalytic Activity of TiO2 Nanoparticles for Photochemical Oxidation of Concentrated Chlorophenols under Direct Solar Radiation." *Int. J. Electrochem. Sci* 7:4871-4888.

Baheiraei, Nafiseh, Fathollah Moztarzadeh, and Mehdi Hedayati. 2012. "Preparation and antibacterial activity of Ag/SiO_2 thin film on glazed ceramic tiles by sol–gel method." *Ceramics International* 38 (4):2921-2925.

Bender, Joel R, and John G Hadley. 1994. "Glass fiber manufacturing and fiber safety: the producer's perspective." *Environmental health perspectives* 102 (Suppl 5):37.

Callister, William D, and David G Rethwisch. 2012. *Fundamentals of materials science and engineering: an integrated approach*: John Wiley & Sons.

Campbell Jr, Flake C. 2003. *Manufacturing processes for advanced composites*: Elsevier.

Chandramohan, D, and K Marimuthu. 2011. "Characterization of natural fibers and their application in bone grafting substitutes." *Acta of Bioengineering & Biomechanics* 13 (1).

Davies, Richard L, and Samuel F Etris. 1997. "The development and functions of silver in water purification and disease control." *Catalysis Today* 36 (1):107-114.

Feng et.al. 2000. 'A mechanistic study of the antibacterial effect of silver ions on Escherichia coli and staphylococcus aureus.' John Wiley & Send.Inc :662-667

Fu, Guifen, Patricia S Vary, and Chhiu-Tsu Lin. 2005. "Anatase TiO2 nanocomposites for antimicrobial coatings." The Journal of Physical Chemistry B 109 (18):8889-8898.

Fujishima, Akira, Tata N Rao, and Donald A Tryk. 2000. "Titanium dioxide photocatalysis." Journal of Photochemistry and Photobiology C: Photochemistry Reviews 1 (1):1-21.

Guzman, Maribel, Jean Dille, and Stéphane Godet. 2012. "Synthesis and antibacterial activity of silver nanoparticles against gram-positive and gram-negative bacteria." Nanomedicine: Nanotechnology, Biology and Medicine 8 (1):37-45.

Hanemann, T. 2006. "Viscosity change of unsaturated polyester–alumina-composites using polyethylene glycol alkyl ether based dispersants." Composites Part A: Applied Science and Manufacturing 37 (11):2155-2163.

Hilonga, Askwar, Jong-Kil Kim, Pradip B Sarawade, Dang Viet Quang, Godlisten Shao, Gideon Elineema, and Hee Taik Kim. 2012. "Silver-doped silica powder with antibacterial properties." Powder Technology 215:219-222.

Hull, Derek, and TW Clyne. 1996. An introduction to composite materials: Cambridge university press.

Kenawy, El-Refaie, SD Worley, and Roy Broughton. 2007. "The chemistry and applications of antimicrobial polymers: a state-of-the-art review." Biomacromolecules 8 (5):1359-1384.

Khan, Mohd Abdul Majeed, Sushil Kumar, Maqusood Ahamed, Salman A Alrokayan, and Mohammad Saleh AlSalhi. 2011. "Structural and thermal studies of silver nanoparticles and electrical transport study of their thin films." Nanoscale research letters 6 (1):1-8.

Kim, Jun Sung, Eunye Kuk, Kyeong Nam Yu, Jong-Ho Kim, Sung Jin Park, Hu Jang Lee, So Hyun Kim, Young Kyung Park, Yong Ho Park, and Cheol-Yong Hwang. 2007. "Antimicrobial effects of silver nanoparticles." Nanomedicine: Nanotechnology, Biology and Medicine 3 (1):95-101.

Kim, Soo-Hwan, Hyeong-Seon Lee, Deok-Seon Ryu, Soo-Jae Choi, and Dong-Seok Lee. 2011. "Antibacterial activity of silver-nanoparticles against *Staphylococcus aureus* and *Escherichia coli*." Korean J Microbiol Biotechnol 39 (1):77-85.

Lellouche, Jonathan, Alexandra Friedman, Jean-Paul Lellouche, Aharon Gedanken, and Ehud Banin. 2012. "Improved antibacterial and antibiofilm activity of magnesium fluoride nanoparticles obtained by water-based ultrasound chemistry." Nanomedicine: Nanotechnology, Biology and Medicine 8 (5):702-711.

Li, Ji Rui. 2012. "Silver-Coated Zinc Oxide Antibacterial Nanocomposite Preparation and Characterization." Advanced Materials Research 383:3823-3827.

Liu, Y, L He, A Mustapha, H Li, ZQ Hu, and M Lin. 2009. "Antibacterial activities of zinc oxide nanoparticles against Escherichia coli O157: H7." Journal of applied microbiology 107 (4):1193-1201.

Malhotra, Sant Kumar, Koichi Goda, and Meyyarappallil Sadasivan Sreekala. 2012. "Part One Introduction to Polymer Composites."

Mayer, C, X Wang, and M Neitzel. 1998. "Macro-and micro-impregnation phenomena in continuous manufacturing of fabric reinforced thermoplastic composites." Composites Part A: Applied Science and Manufacturing 29 (7):783-793.

Mazumdar, Sanjay K. 2001. *Composites Manufacturing - Materials, Product and Process Engineering*. CRC Press.

Michael L. Shuler, Fikret Kargi. 2002. Bioprocess Engineering, Second Edition: The National Academies Press.

Montazer, Majid, Amir Behzadnia, Esfandiar Pakdel, Mohammad Karim Rahimi, and Mohammad Bameni Moghadam. 2011. "Photo induced silver on nano titanium dioxide as an enhanced antimicrobial agent for wool." Journal of Photochemistry and Photobiology B: Biology 103 (3):207-214.

Muñoz-Bonilla, Alexandra, and Marta Fernández-García. 2012. "Polymeric materials with antimicrobial activity." Progress in Polymer Science 37 (2):281-339.

Pucić Irina and Ranogajec Franjo. 2003. "Phase separation during radiation crosslinking of unsaturated polyester resin. " Radiation Physics and Chemistry 67 (3): 415-419

Raffi, M, F Hussain, TM Bhatti, JI Akhter, A Hameed, and MM Hasan. 2008. "Antibacterial characterization of silver nanoparticles against *E. coli* ATCC-15224." Journal of Materials Science and Technology 24 (2):192-196.

Rao, Yuanyuan, Wei Wang, Fatang Tan, Yuncheng Cai, Junwen Lu, and Xueliang Qiao. 2013. "Influence of different ions doping on the antibacterial properties of MgO nanopowders." Applied Surface Science 284:726-731.

Ravishankar Rai, V, and A Jamuna Bai. 2011. "Nanoparticles and their potential application as antimicrobials." Science against microbial pathogens: Communicating current research and technological advances, A. Méndez-Vilas (Ed.):197-209.

Ren, Ling, Xiao Lin, Lili Tan, and Ke Yang. 2011. "Effect of surface coating on antibacterial behavior of magnesium based metals." Materials Letters 65 (23):3509-3511.

Shaw, Andrew, Srinivas Sriramula, Peter D Gosling, and Marios K Chryssanthopoulos. 2010. "A critical reliability evaluation of fibre reinforced composite materials based on probabilistic micro and macro-mechanical analysis." Composites Part B: Engineering 41 (6):446-453.

Sondi, Ivan, and Branka Salopek-Sondi. 2004. "Silver nanoparticles as antimicrobial agent: a case study on *E. coli* as a model for Gram-negative bacteria." Journal of colloid and interface science 275 (1):177-182.

Srivastava, A, A Majumdar, and BS Butola. 2012. "Improving the Impact Resistance of Textile Structures by using Shear Thickening Fluids: A Review." Critical Reviews in Solid State and Materials Sciences 37 (2):115-129.

Tan, VBC, TE Tay, and WK Teo. 2005. "Strengthening fabric armour with silica colloidal suspensions." International Journal of Solids and Structures 42 (5):1561-1576.

Thamaphat, Kheamrutai, Pichet Limsuwan, and Boonlaer Ngotawornchai. 2008. "Phase characterization of TiO2 powder by XRD and TEM." Kasetsart J.(Nat. Sci.) 42:357-361.

Xie, Yanping, Yiping He, Peter L Irwin, Tony Jin, and Xianming Shi. 2011. "Antibacterial activity and mechanism of action of zinc oxide nanoparticles against Campylobacter jejuni." Applied and environmental microbiology 77 (7):2325-2331.

Xue, Xiangxin, Yuzheng Wang, and He Yang. 2013. "Preparation and characterization of boron-doped titania nano-materials with antibacterial activity." Applied Surface Science 264:94-99.

Yoshida, Y, Kenichi Shirai, Y Nakayama, M Itoh, M Okazaki, H Shintani, S Inoue, Paul Lambrechts, Guido Vanherle, and Bart Van Meerbeek. 2002. "Improved filler-matrix coupling in resin composites." Journal of dental research 81 (4):270-273.

Zhang, Erlin, Fangbing Li, Hongying Wang, Jie Liu, Chunmin Wang, Muqin Li, and Ke Yang. 2013. "A new antibacterial titanium–copper sintered alloy: Preparation and antibacterial property." Materials Science and Engineering: C 33 (7):4280-4287.

Zibaii, Mohammad Ismail, Hamid Latifi, Zahra Saeedian, and Zinab Chenari. 2014. "Nonadiabatic tapered optical fiber sensor for measurement of antimicrobial activity of silver nanoparticles against *Escherichia coli*." Journal of Photochemistry and Photobiology B: Biology 135:55-64.